J. Fluid Mech. (2014), *vol.* 754, *pp.* 39–74.
doi:10.1017/jfm.2014.377

Tollmien–Schlichting wave growth over spanwise-periodic surface patterns

Robert S. Downs III† and Jens H. M. Fransson

Linné Flow Centre, KTH Mechanics, SE-10044 Stockholm, Sweden

(Received 19 November 2013; revised 20 May 2014; accepted 25 June 2014;
first published online 30 July 2014)

A novel type of surface roughness is deployed in a zero-pressure-gradient boundary layer with the goal of delaying the onset of laminar-to-turbulent transition for drag reduction purposes. This proof-of-concept experiment relies on forcing phase-triggered Tollmien–Schlichting (TS) waves across a range of initial amplitudes to produce amplified boundary-layer disturbances in a controlled and repeatable manner. Building on earlier work demonstrating attenuation of forced disturbances and delay of transition with spanwise arrays of discrete roughness and miniature vortex generators (MVGs), the present work seeks a roughness shape which might find success in a wider range of flows. Toward that end, streamwise-elongated humps are regularly spaced in the spanwise direction to form a wavy wall. By direct modulation of the mean flow, growth rates of the forced disturbances are increased or decreased, depending on the roughness configuration. Boundary-layer velocity measurements with hot-wire probes have been performed in a parametric study of the effects of roughness-field geometry and forcing amplitude on TS-wave growth and transition. The roughness field proves detrimental to passive flow control efforts in some configurations, while a reduction in the TS-wave amplitudes compared with the smooth-wall reference case is observed at other conditions. Substantial delays in the onset of transition are demonstrated when TS waves are forced with large amplitudes.

Key words: boundary-layer stability, boundary-layer control

1. Introduction

A longstanding goal of flow control research is development of drag-reducing devices. Currently, the greatest potential for reducing fuel consumption of modern aircraft lies with advancing laminar flow control (LFC) technology (Green 2008). The optimist will note that many LFC techniques exist in various stages of development. The practical difficulties associated with active systems (e.g. boundary-layer suction) have thus far limited use of these systems to the laboratory or flight tests, despite promising results in these environments. Passive systems, however, have an advantage in that they are more mechanically simple and require no energy input. The low-roughness surface finish found on some aircraft can be considered a simple

† Email address for correspondence: downs@mech.kth.se

passive drag-reducing device, as transition is significantly advanced by surface roughness in some scenarios (Saric, Carpenter & Reed 2011). Another strategy for passively reducing skin-friction drag is the application of riblets. Rather than delaying the onset of transition, these streamwise-oriented, spanwise-periodic surfaces ameliorate the high wall shear stress in turbulent boundary layers. The relevant literature still hosts some debate concerning the exact nature of the mechanism (García-Mayoral & Jiménez 2011*a*). The goal of the present work is to effect a transition delay for drag reduction by introduction of controlled modulation to the boundary-layer velocity field. To do so, a patterned field of surface roughness not unlike that of riblets is employed.

Although a complete understanding of surface-roughness-induced boundary-layer transition eludes the grasp of contemporary researchers, this field of study is far from stagnant. For many years, the prevailing notion was that roughness had, at best, a neutral effect on transition. The empirical correlations developed in the early period of transition research remain useful guides in some scenarios. The roughness-height-based Reynolds number is a common metric, defined as $Re_k = U(k)k/\nu$, where $U(k)$ is the theoretical undisturbed streamwise velocity at the roughness height, k, and ν is the kinematic viscosity. For artificial distributed roughness, a critical roughness-height-based Reynolds number of $Re_{k,crit} = 600$ was observed in the experiments of von Doenhoff & Horton (1958). Klebanoff, Cleveland & Tidstrom (1992) report that $Re_{k,crit} = 325$ for discrete hemispherical roughness elements, while $Re_{k,crit} = 450$ for cylindrical roughness. The value of $Re_{k,crit}$ varies somewhat with roughness shape and experimental facility. The inability of simple correlations to reconcile observed variations in instability growth and transition location prompted Morkovin (1969) to elucidate the importance of branching paths connecting receptivity and breakdown to turbulence. For roughness of subcritical height, transient growth theory describes the evolution of the induced disturbances, i.e. a period of spatial growth followed by exponential decay (see e.g. Reshotko 2001). The physical mechanism of this phenomenon was described by Landahl (1980) as the re-distribution of high- and low-momentum fluid near the wall by streamwise vortices, and is often referred to as the lift-up mechanism. This accounts for the flow deformation in the far wake of the roughness and the decaying disturbances. The connection of transient growth theory with roughness-induced transition has renewed efforts to form a fundamental understanding of this process and the amount of recent literature on the subject is considerable.

Despite the detrimental influence of roughness-induced disturbances on boundary-layer stability in many flows, deliberately designed discrete roughness elements can delay transition in boundary layers dominated by crossflow (Saric *et al.* 2011) or streamwise instabilities (Fransson *et al.* 2006). An interesting possibility for flat-plate boundary layers is raised by the work of Kosorygin, Radeztsky & Saric (1995), in which selectively placed two-dimensional roughness elements scatter acoustic disturbances into two-dimensional waves which subsequently undergo destructive interference. In the crossflow scenario, the primary instability leading to transition is manifested as streamwise-oriented vortices that produce spanwise-periodic deformation of the mean flow. The wavenumber spectrum of the stationary disturbances can be initiated with spanwise-periodic arrays of roughness applied at the first crossflow neutral stability point. The roughness elements are small: heights of approximately 10 μm raise the initial disturbance above that of naturally occurring perturbations and at relevant test conditions, $Re_k \approx 0.2$. When a short-wavelength disturbance whose growth rate is less than that of the naturally occurring instability is excited,

growth of the most amplified mode is suppressed and significant delays in transition may be realized. Though sensitive to environmental conditions, this method of roughness-induced transition delay has been successfully demonstrated in low-speed (Saric, Carrillo & Reibert 1998) and high-speed (Schuele, Corke & Matlis 2013) boundary layers.

Patterns of discrete surface roughness elements can be applied to delay transition due to viscous shear-layer instabilities, i.e. Tollmien–Schlichting (TS) waves. For the case of a two-dimensional flat-plate boundary layer without a streamwise pressure gradient, the transition scenario proceeding through linear instability growth follows this path. The primary instability takes the form of a travelling wave which can be two-dimensional or oblique. The more-amplified two-dimensional TS waves are the model disturbance of the present work. The strength of this instability may be characterized by the temporal root-mean-square of the streamwise fluctuating velocity, u'_{rms}. A general criterion for growth of fundamental secondary instabilities requires sufficiently large TS-wave amplitudes with $u'_{rms,max} \geqslant 0.01U_\infty$, where U_∞ is the free-stream velocity. Secondary instability of TS waves is evident as spanwise modulations of the flow, or so-called Λ vortices. In one possible transition scenario, high-frequency turbulent bursts (a harbinger of transition) are observed within a few TS wavelengths of the emergence of fundamental secondary instabilities. These bursts appear intermittently at first, with increasing length and frequency of occurrence as the flow proceeds through breakdown to fully turbulent (Klebanoff, Tidstrom & Sargent 1962; Herbert 1988). This type of scenario is usually associated with temporal amplitude and phase modulations of the primary instability resulting from natural background disturbances (Kachanov 1994). TS waves that are only weakly modulated are observed to produce a more gradual transition, devoid of turbulent spots (Borodulin *et al.* 2002*a*). Although the path to transition will deviate through transient growth or bypass mechanisms in the presence of sufficiently large roughness or elevated free-stream turbulence (Saric, Reed & Kerschen 2002), the present work focuses on linear instability growth as the reference case.

2. Background

Previous experimental and numerical studies have collectively proven that a delay of TS-wave-induced transition may be achieved by introducing controlled disturbances which inhibit growth of the primary instability. In the Floquet analysis of Cossu & Brandt (2004), steady disturbances were imposed on a zero-pressure-gradient boundary layer, chosen such that they experience maximum spatial growth. These so-called optimal disturbances (Andersson, Berggren & Henningson 1999; Luchini 2000) are conceptualized as a spanwise series of streamwise vortices which in turn produce streamwise streaks via the lift-up mechanism. The dimensionless spanwise wavenumber of the optimal disturbances is $\beta = 2\pi\delta/\lambda = 0.45$, where λ is the spanwise wavelength, and $\delta = \sqrt{\nu x/U_\infty}$, with x denoting the downstream distance from the leading edge. These streaks can reach amplitudes as large as 26 % of U_∞ before secondary instabilities arise (Andersson *et al.* 2001). Streak amplitude may follow several definitions; in general, it measures the steady deviation of the flow from the two-dimensional reference boundary-layer velocity. The definition used by Andersson *et al.* (2001) was the average of the maximum and minimum deviations from a Blasius boundary layer. Cossu & Brandt (2004) showed that formerly two-dimensional TS waves modulated by optimal streaks grow more slowly than unmodified TS waves. A physical interpretation of this phenomenon was found in the perturbation kinetic

energy equation. Viscous dissipation is of negative sign and thus always contributes to energy decay. The wall-normal and spanwise production terms, $\overline{u'v'}(\partial U/\partial y)$ and $\overline{u'w'}(\partial U/\partial z)$ respectively, may assume either sign. In a two-dimensional boundary layer, the latter is zero as the spanwise derivative vanishes by definition. When optimal streaks were imposed under these conditions, it was observed that $\overline{u'w'}$ and $\partial U/\partial z$ had opposing odd symmetry about streak centrelines and thus had a net negative contribution to the perturbation kinetic energy. It was further demonstrated that higher-amplitude streaks have a greater stabilizing effect as a result of the higher spanwise shear.

Experimental observation of TS-wave stabilization with boundary-layer streaks was made by Fransson *et al.* (2005*a*). Spanwise arrays of cylindrical roughness elements were employed to produce streaks within a flat-plate boundary layer, and streak amplitudes of approximately 12 % of U_∞ were measured in these experiments. An instability associated with the unsteady flow in the roughness wakes prevented higher streak amplitudes. It is recognized (White 2002; Fransson *et al.* 2004) that the character of roughness-induced streaks differs from that of optimal disturbances and that the former may be considered sub-optimal disturbances. Denissen & White (2013) showed that roughness-induced disturbances are more effective instigators of transition than optimal disturbances, due to the more unstable mid-wake region. Thus, optimal perturbations may not represent the 'worst case' for transition. Fransson *et al.* (2005*a*) showed that even with the streak amplitude limited to less than half of that expected for inflectional instability of the streaks themselves, the modification of the boundary layer was sufficient to attenuate the growth of TS waves. Spanwise-modulated TS-like disturbances across a range of frequencies experienced lower growth rates than their two-dimensional reference counterparts. In that experiment, growth rates were computed by integrating streamwise–normal planes of disturbance amplitudes to account for three-dimensionality of the TS waves.

Additionally, the disparity between TS-wave amplitudes at the apex of their growth in the two-dimensional and streaky boundary layers increased with roughness height. That is, comparison of TS-wave amplitudes measured in streaky boundary layers with those measured at the upper branch of the neutral stability curve for Blasius flow (the branch II location) demonstrates that higher-amplitude streaks more effectively reduced the TS-wave growth rates in those experiments. Using this technique in concert with moderate-amplitude TS waves, a substantial delay in the onset of transition was achieved in the experiments of Fransson *et al.* (2006). In addition, when broadband noise was used as an excitation source instead of single-frequency forcing, transition was also delayed, albeit by a shorter distance.

Another experimental effort aimed at TS-wave suppression in streaky boundary layers was conducted by Gürün & White (2005). TS waves were generated using acoustic forcing in the free stream and two-dimensional roughness to scatter the convected disturbances into TS wavelengths, and arrays of cylindrical surface roughness upstream of the two-dimensional roughness provided mean-flow modulation. The modulated boundary layer was less receptive to acoustic disturbances, and the growth rates of unsteady disturbances were also reduced. Thus, moderate changes to the breakdown location may be attributed to reduced receptivity of the streaky boundary layer in those experiments.

The aforementioned experiments and simulations establish that streamwise-streak amplitude can be optimized for stabilization purposes. Using solutions of the nonlinear parabolized stability equations validated against direct numerical simulations (DNS), Bagheri & Hanifi (2007) examined the effect that streak wavelength plays in TS-wave

damping. As the optimal disturbance is one that by definition experiences the maximum growth, suboptimally spaced disturbances were initiated with larger values such that all streaks attained an amplitude of 10 %. For a set of such streaks with wavenumbers $0.1 \leqslant \beta \leqslant 1.0$, TS-wave growth rates were minimized when the steady streaks reached their maximum amplitudes near the first neutral stability point, x_I. For the tested conditions, the most effective streaks had $\beta \approx 0.6$. Further numerical investigation of the control mechanism was undertaken by Schlatter *et al.* (2010) via large-eddy simulations. Apart from TS waves, other types of disturbances were imposed on the streaky boundary layer. A delay of TS-wave-dominated transition was observed when the disturbances were single-frequency two-dimensional waves or spanwise-invariant random noise. The streak control mechanism was not effective in the case of oblique waves and free-stream turbulence, i.e. disturbances with significant three-dimensional character. In that study, it was found that the streaks were more effective when their wavelengths were longer than those of the naturally arising secondary instability modes. While the effectiveness of high-amplitude streaks in attenuating TS-wave growth rates was confirmed, interaction between low-amplitude streaks (2.6–5 %) and TS waves excited the first harmonic of the imposed streaks. A numerical stability analysis performed by Liu, Zaki & Durbin (2008) explored the effect of streak wavelength on primary and secondary instabilities in TS-wave-dominated transition. A key result was that while streaks of long and short wavelength reduced TS-wave growth, they also amplified secondary instabilities (Λ vortices). If the streaks were spaced at approximately the same wavelength as the secondary instability, interaction between the two produced a net loss of laminar flow, whereas detuning this interaction allowed a transition delay.

One advantage of such numerical investigations is the possibility of direct specification of the boundary-layer streaks at the inlet of the computation domain. Any practical application of this stabilizing mechanism will, of course, require some physical provision to generate streaks. A conventional method of doing so employs spanwise arrays of cylindrical surface roughness, as discussed previously. The shortcoming of this approach is an early promotion of transition at moderate Reynolds numbers due to instabilities associated with the unsteady wake. The high-amplitude streaks desired for more effective control cannot be generated with such roughness. A solution to this problem was found by Fransson & Talamelli (2012) in miniature vortex generators (MVGs). Whereas vortex generators are usually employed for separation control, MVGs with heights h of the order of $\delta_{99}/2$ were used to create strong streamwise vorticity while avoiding the problems associated with bluff surface roughness. It was demonstrated that the MVGs tested have $Re_{k,crit} = 547$, compared with $Re_{k,crit} = 422$ for cylindrical surface roughness in a similar configuration (Fransson *et al.* 2005*a*). The importance of $Re_{k,crit}$ is as a measure of robustness in generating streaks in a stable manner. For Reynolds numbers above the critical value, the onset of transition moves sharply forward, thereby imposing a drag penalty that is larger than in the unmodified boundary layer. This underlines the challenge of exploiting this mechanism for drag reduction: relatively high-amplitude streaks are required without exceeding the critical speeds or roughness heights that would promote an early transition through a bypass mechanism. Furthermore, $Re_{k,crit}$ is determined empirically and is sensitive to roughness shape and experimental set-up.

In the experiments of Fransson & Talamelli (2012), stable streaks with amplitudes as high as 32 % were created using MVGs. The amplitude of the streaks grew sharply in the wake of the MVGs, reached a maximum approximately $50h$ downstream and decayed thereafter. The possibility of reinforcing the streaks with a second

array of MVGs offers a tenable solution to the problem of maintaining a streaky base flow. Building upon this work, Shahinfar *et al.* (2012) tested the efficacy of MVGs for delaying TS-wave-induced transition. A substantial delay in the onset of transition was achieved and the transitional Reynolds number was at least doubled. The eventual transition location in the controlled case was not specified since it took place downstream of the measurement region. Drag due to skin friction was estimated from velocity profile measurements and revealed at least a 22 % improvement over unmodified flow. Although not optimized for transition control, the MVGs were sensibly chosen. The streak amplitudes reached their maxima near the lower branch of the neutral stability curve for Blasius flow, x_I (the branch I location), and had $\beta = 0.30$. It is that study and the recent works of Shahinfar *et al.* (2013) and Shahinfar, Sattarzadeh & Fransson (2014) in particular which have prompted the present work.

The effectiveness of spanwise arrays of roughness and MVGs for transition delay has been convincingly demonstrated in experiments and numerical analyses, and an explanation for the stabilizing mechanism has been given (Cossu & Brandt 2004). In the present work, a regularly patterned and aerodynamically simple type of surface roughness is developed and its potential for modifying TS-wave-induced transition is tested. Rather than exploiting the lift-up mechanism to produce streamwise streaks, the boundary layer is modulated directly by introducing spanwise periodicity to the wall. This is accomplished with humps elongated in the streamwise direction, and arrayed regularly in the spanwise direction. The requisite spanwise shear ($\partial U/\partial z$) is introduced and destabilization related to roughness wakes is minimized. As opposed to MVGs, the roughness has a constant cross-section shape, except where the leading and trailing edges are smoothly ramped to the plate surface. The shape also avoids the sharp edges found in arrays of cylindrical roughness, in an effort to reduce the influence of wake-related instability on the flow. The design of this regularly patterned field of surface features is advantageous for the immediate purpose of these experiments, and is also attractive from a practical view. Such a shape is amenable to manufacturing; it could, for instance, be stamped into the aluminium skin of an aircraft wing. In addition, the shape of the roughness is chosen to give some insight into the nature of the stabilizing mechanism, by modulating the mean flow without producing the strong streamwise-oriented vortices that accompany more conventional surface roughness elements.

The similarity of this surface with riblets must be considered. A wide body of research exists concerning the application of riblets for drag reduction in turbulent boundary layers. The cross-section shape of riblets is typically triangular, with optimal drag reduction achieved with spacing $s^+ \approx 16$ in viscous wall units and height $h \approx 0.5s$ (Bechert *et al.* 1997). Here, $s^+ = s(\sqrt{\tau_w/\rho})/\nu$, where τ_w is the wall shear stress and ρ is the density. For commonly encountered conditions, riblet heights and wavelengths are in the sub-millimetre range. Conversely, the roughness designed for transition delay using the streak stabilization method typically has $\lambda/h > 10$, with h of the order of 1 mm. It is well-established that riblets do reduce skin-friction drag in turbulent boundary layers. The effect of riblets on turbulent boundary-layer flow is described in detail by García-Mayoral & Jiménez (2011*b*). The concept of different virtual origins for streamwise and spanwise flow components accounts for drag reduction by impeding turbulent mixing of streamwise momentum near the wall. As riblet size is increased, drag also increases due to formation of rotating flow structures aligned in the spanwise direction which are susceptible to a Kelvin–Helmholtz-like instability. Additionally, García-Mayoral & Jiménez (2011*a*) note that riblet-aided watercraft have been successful in some sporting events but the contribution of the riblets cannot be quantified.

Several investigations of riblets' effect on stability and laminar–turbulent transition have been completed. The experiments of Ladd *et al.* (1993) focused on natural transition and found that riblets applied to a flat plate enhance transition when $Re_k > 6$. Luchini & Trombetta (1995) performed simulations and a stability analysis which showed that TS-wave growth rates were increased over the grooved riblet surface, and attributed this to the increased flow rate between riblets. A comprehensive experimental investigation of the stability of zero-pressure-gradient boundary layers in the presence of riblets was performed by Grek *et al.* (1995) and Grek, Kozlov & Titarenko (1996). In the former, streamwise vortices were created upstream of the riblets with an array of roughness elements. The riblets effectively suppressed the streamwise vorticity and the flow was more spanwise uniform. The latter series of experiments focused on interactions between artificially excited TS waves and riblets in a laminar boundary layer. The TS-wave growth rates were increased over the riblet surface, in agreement with earlier experiments. However, the formation of turbulent spots further downstream was inhibited by the presence of riblets. Klumpp, Meinke & Schröder (2010) performed simulations of a similar flow configuration and observed that there was no significant change in transition location with riblets. The detailed measurements of Litvinenko *et al.* (2006) showed that riblets can prevent the formation of turbulent spots from Λ vortices, and the DNS of Strand & Goldstein (2011) showed that when turbulent spots are formed, the spreading angle is constrained by riblets. Thus, although riblets participate in the development of primary and secondary instabilities in flat-plate boundary layers, their net effect on transition is not large in most circumstances.

Surface patterns other than riblets have been used to modify boundary-layer flows. Random, distributed surface roughness can increase TS-wave growth rates by enhancing the three-dimensionality of the waves (Corke, Bar-Sever & Morkovin 1986) and appears to accelerate the onset of secondary instability. Nugroho, Hutchins & Monty (2013) demonstrated that spanwise periodicity may be imposed on a turbulent boundary layer with riblet plates of opposing oblique angles which form a 'herringbone' pattern. Surface features on a larger scale have been tested by Zverkov, Zanin & Kozlov (2008). A wing with a spanwise-wavy surface was designed for separation control and it was observed that separation was prevented on the peaks, but promoted in the valleys. The flow was presumably stabilized by the favourable pressure gradient over the peaks. In the valleys, however, inflectional velocity profiles and amplified high-frequency disturbances were observed. Similar surface features can also appear in practical scenarios. Garzon & Roberts (2013) described a test aircraft in which sealant deterioration on the wing produced a surface wave which destabilized the boundary layer, leading to an earlier transition. Thus, the scale and shape of surface features broadly classified as roughness, as well as the character of the flow, clearly influence the effect of roughness on boundary-layer flows. Although the complicated nature of the interaction prevents simple correlations, it admits the possibility that sensibly chosen roughness can exploit known stabilizing mechanisms.

Apart from steady streaks induced by discrete surface features or roughness, qualitatively similar deformations to mean flow in two-dimensional boundary layers can result from Görtler vortices. Arising from a centrifugal instability in boundary-layer flow over concave surfaces (Saric 1994), these streamwise vortices can also interact with TS waves in significant ways. It has long been recognized that boundary-layer stability may be affected by spanwise variations in mean flow due to Görtler vortices (Nayfeh 1981). The triple-deck analysis by Hall & Bennett (1986) demonstrated that TS waves and Görtler vortices may interact in a manner

such that the former increases the growth rates of the latter, when the TS waves have large wavenumbers. An early analysis of TS wave and Görtler vortex interaction was undertaken by Nayfeh & Al-Maaitah (1988), who generalized their approach to a generic series of streamwise vortices. Although limited to small-amplitude TS waves which do not influence Görtler-vortex growth rates, it was observed that these vortices increase TS-wave growth rates at low frequencies ($F = 25$–55). These results were complemented by those of Bennett & Hall (1988). That study showed that although small-amplitude Görtler vortices could act to further increase growth rates of unstable TS waves, there was little change to the evolution of neutral TS waves. Further numerical investigations have shown increased growth rates for oblique TS waves when their wavelengths are half those of the Görtler vortices (Malik & Hussaini 1990). The simulations of Mendonça, Morris & Pauley (2000) are more relevant to the present work, in that Görtler vortices and TS waves of comparable amplitudes are investigated and found to strongly interact. Importantly, TS-wave damping is observed when mean-flow distortion and Görtler-vortex amplitudes grow to values of the order of $0.01U$ and $0.1U$, respectively. This phenomenon is also observed when the mean-flow distortion mode is not affected by interactions of Görtler vortices and TS waves. When the Görtler-vortex growth rates are maximized (with spanwise wavenumber $\beta = 0.5$), TS-wave damping is likewise maximized. Although transition was not modelled in that work, rapidly growing harmonics were construed as a precursor to transition advanced by amplified Görtler vortices. In the context of the present work, however, it seems that amplification of moderate- to large-amplitude TS waves can falter in the presence of significant spanwise variations in mean flow arising in different ways.

With this knowledge in hand, the present experiments use a regularly patterned field of surface roughness to influence the stability of a quasi-zero-pressure-gradient boundary layer. The roughness bears some resemblance to riblets, but the height, cross-section and spanwise spacing are selected based on the success of roughness used to generate streaky boundary layers for control of streamwise instabilities. TS waves are forced to create a well-controlled, phase-triggered disturbance for the purpose of a careful quantitative study. Although these disturbances are somewhat unrealistic, that TS waves of random phase were measured in flight over a two-dimensional wing by Peltzer (2008) indicates that they are an important facet of natural transition. Receptivity of background disturbances, however, will play a role in the transition process. Forcing strong disturbances defers the question of natural receptivity. Growth of the primary instability is measured to assess the effect of streamwise roughness on boundary-layer stability, while transition location measurements provide a practical metric of passive control efficacy.

3. Experimental method

The zero-pressure-gradient flat-plate boundary layer is a prototypical platform of stability experiments. Many of the techniques on which the present work relies were validated in previous experiments. The facility utilized is the minimum-turbulence-level (MTL) wind tunnel at KTH Royal Institute of Technology, and meets the recommended criteria for stability experiments (Reshotko, Saric & Nagib 1997). The wind tunnel forms a closed circuit, and is temperature-controlled. The test section is 7 m long with a rectangular cross-section of 1.2 m $\times$ 0.8 m. A full account of the most recent flow-quality measurements was given by Lindgren & Johansson (2002). The key points are that the streamwise and transverse turbulence intensities are less

than 0.025 % and 0.035 %, respectively, at relevant test speeds, with static pressure fluctuations $p' \leqslant \pm 0.06\,\%$. The free-stream turbulence intensity in the test section is close to that of the low-turbulence flight environment (Riedel & Sitzmann 1998). Even though the scale and frequency-domain distribution of wind-tunnel free-stream disturbances are distinct from those of an atmospheric free stream, the development of disturbances leading to transition in the boundary layer is expected to qualitatively represent that which could be observed in flight. That is, the low-intensity free-stream turbulence will not significantly affect instability growth or transition due to forced TS waves. Given the ease with which environmental conditions may influence the transition process, a detailed description of the experimental set-up is warranted.

3.1. *Experimental set-up*

The boundary layer of the present experiments develops on a 6.2 m long flat aluminium plate which spans the 1.2 m width of the test section. The 160 mm long asymmetric leading edge is designed to reduce the size of the pressure recovery region, facilitating a rapid return to zero-pressure-gradient flow. A 1.5 m long hinged trailing-edge flap is used to place the stagnation location on the test side of the plate. To allow access by the probe traversing system, the plate is suspended horizontally in the test section at a unit height of 0.30. This location is also sufficiently far from the centreline, where nodes of large-scale rotational motion may exist (Saric 2007). The externally mounted traversing system positions hot-wire probes in an approximate measurement volume (x, y, z) of 4500 mm × 150 mm × 145 mm with precision of the order of microns, where these coordinates denote the streamwise, wall-normal, and spanwise directions respectively. In the present experiments, all boundary-layer measurements are made using hot-wire probes whose sensing elements have length 0.7 mm and diameter 2.54 μm, with overheat ratios set to 1.5. Temporal response rates are consistently in the vicinity of 30 kHz. The probes are calibrated in the wind-tunnel stream using the modified version of King's law from Johansson & Alfredsson (1982), across the range 0–18 m s^{-1}.

A boundary layer formed in the absence of a streamwise pressure gradient has a well-understood and defined solution. It is also a singular test point, the figurative watershed of viscous instability growth. In practice, attaining this condition requires some care. Six jointed panels comprise the test section ceiling and fine adjustments of threaded mounts allow iterative tailoring of the streamwise pressure gradient. Although the desired accuracy in measuring the pressure gradient precludes direct measurement with manometers, boundary-layer velocity measurements are sufficient. Using a reference pressure and velocity with an application of Bernoulli's law leads to an expression for the coefficient of pressure as $C_p = 1 - (U_e/U_\infty)^2$, where U_e is the boundary-layer edge velocity. A more sensitive indicator of the pressure gradient is comparison of the boundary-layer shape factor, $H = \delta^*/\theta$, to its theoretical value for a zero-pressure-gradient boundary layer: $H = 2.591$, where δ^* and θ are the displacement and momentum thicknesses. Experimental measurements of this quantity are obtained from velocity profiles via numerical evaluation of the respective integral relations for δ^* and θ.

These quantities are measured at the primary test speed of $U_\infty = 12$ m s^{-1} and plotted in figure 1. The pressure rise and subsequent recovery associated with the leading edge of the plate are evident in figure 1(*a*), followed by a long region of approximately zero-pressure-gradient flow from $x = 300$ to 3200 mm. The boundary-layer integral quantities are normalized with δ and plotted with the shape factors in

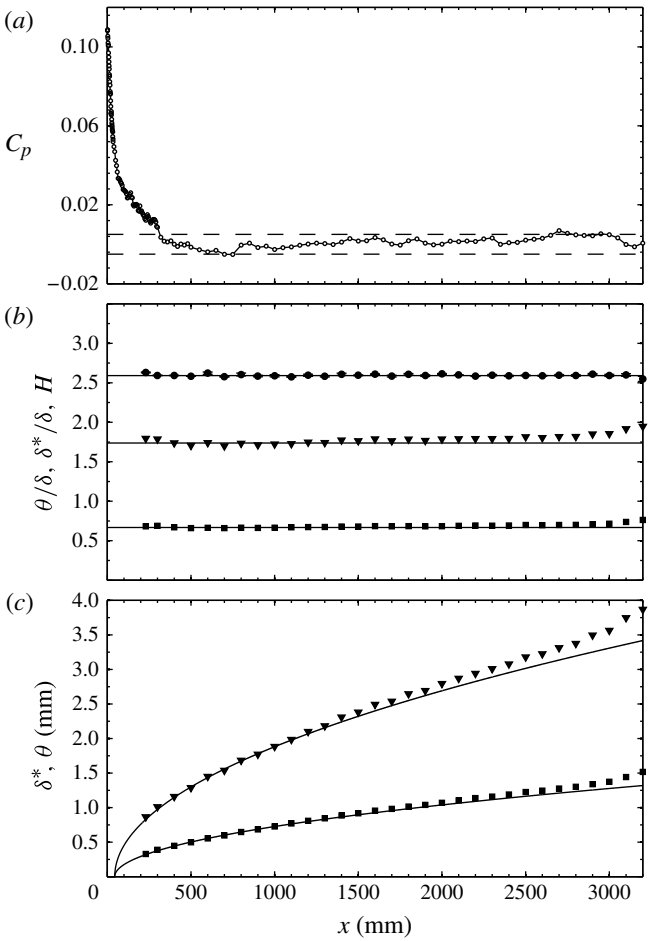

FIGURE 1. Mean flow characteristics at $U = 12$ m s^{-1}. (*a*) Pressure distribution computed as $1 - (U_e/U_\infty)^2$. Dashed lines mark $C_p = \pm 0.005$. (*b*) Measured values of H (●) with normalized δ^* (▼), and θ (■). Error bars represent the standard error of the mean from measurements at five spanwise locations. A solid line marks the theoretical value of $H = 2.591$. For $m = -0.003$, the theoretical values $\delta^*/\delta = 1.74$ and $\theta/\delta = 0.67$ are also marked with solid lines. (*c*) Dimensional values of δ^* (▼) and θ (■) with theoretical zero-pressure-gradient values adjusted for a virtual origin at $x = 44.5$ mm.

figure 1(*b*). Curve fits to measured δ^* and θ are optimized using a virtual leading edge location of $x_{vle} = 44.5$ mm, which is then used to adjust theoretical values of δ. The corresponding dimensional values are plotted in figure 1(*c*). The mean shape factor is $H = 2.60$ and the corresponding Falkner–Skan parameter is $m = -0.003$, indicating a weakly adverse pressure gradient. These values confirm that a suitable test condition is attained. Toward the end of the measurement domain, the shape factor values begin to decrease in advance of the onset of transition. In the present conditions, natural transition is observed between $x = 3200$ and 3300 mm, giving a Reynolds number based on transition location $Re_{x,tr} = 2.6 \times 10^6$.

The basic-state flow is modulated in the spanwise direction using a regular pattern of elongated humps. This roughness pattern is not unlike that of riblets though

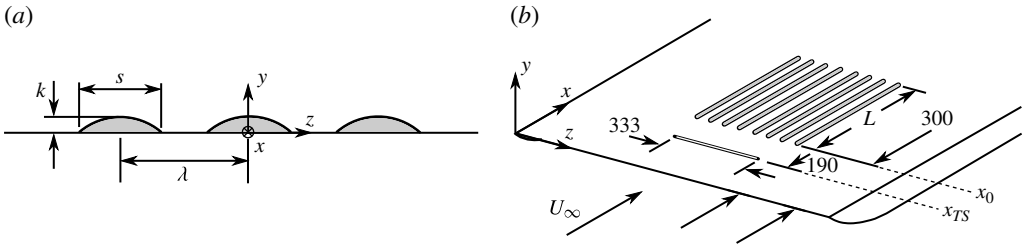

FIGURE 2. Schematic drawings of (*a*) cross-section view of the surface roughness and (*b*) the experimental flat-plate set-up. All dimensions are in mm, not to scale.

$[k\|\lambda\|L]$ (mm)	β	$Re_{k,LE}$	$Re_{k,TE}$
[1|7.5|250]	0.51	424	318
[1|10|250]	0.38	424	318
[1|15|250]	0.26	424	318
[1|15|480]	0.26	424	269
[1|20|250]	0.19	424	318
[1|30|250]	0.13	424	318

TABLE 1. Summary of roughness patterns tested. For all configurations, $x_0 = 300$ mm and $U_\infty = 12$ m s^{-1}.

the scale and cross-section shape vary significantly in comparison. Rather than the triangular cross-sections which are common in riblet designs, the roughness elements of the present experiments present hemispherical caps to the oncoming flow. The roughness is shown schematically in figure 2(*a*). The spanwise width and height of the roughness are held constant at $s = 6$ mm and $k = 1$ mm respectively. The wavelength λ and streamwise length L are varied in these experiments. The shorthand notation $[k|\lambda|L]$ (in mm) is used to specify roughness configurations. The physical roughness elements are cast in a tin alloy and attached directly to the plate using spray adhesive. The leading and trailing edges of the roughness are linearly ramped from the plate surface to k over a length of 10 mm. The humps are placed with their axes parallel to the incoming flow, with the leading edges at $x_0 = 300$ mm relative to the physical leading edge of the plate.

The spanwise wavelength of the roughness pattern is varied using the same roughness elements. That is, λ/s is not constant in these experiments. For a test speed of $U_\infty = 12$ m s^{-1}, the theoretical zero-pressure-gradient value of the boundary-layer thickness at the leading edge of the roughness pattern is $\delta = 0.61$ mm. For this roughness shape, $\lambda_{min} = 6$ mm and thus $\beta_{max} = 0.64$. A summary of configurations tested is given in table 1. In this table, the Re_k values are specified at the leading and trailing edges of the roughness. The dimensionless spanwise wavenumbers comprise a range including that of the optimal disturbance ($\beta = 0.45$) and the $\beta = 0.30$ MVG array used by Shahinfar *et al.* (2012). The roughness height and test speed are chosen to produce moderate deformation of the mean flow, while avoiding a bypass-type transition. This experimental set-up is depicted in figure 2(*b*). Upstream of the roughness pattern, a thin slot is used to excite controlled unsteady disturbances.

3.2. *Controlled unsteady disturbances*

While the ultimate goal of this flow control research is to develop a method to delay the onset of naturally arising transition, the present experiments are an intermediate step in which transition is forced with controlled disturbances. The utility of doing so is twofold: measurements of the primary instability can be phase-locked with the disturbance source, and disturbance growth and transition location are more repeatable. These qualities are a significant benefit to the experimentalist and, in controlling the disturbance conditions, the results become less dependent on the natural free-stream signature of this particular wind tunnel. The importance of generating precisely controlled disturbances in stability and transition experiments is reviewed by Gaponenko & Kachanov (1994). In that work, three methods of introducing controllable disturbances at specific frequencies with minimal mean-flow influence are described. One of these methods employed loudspeakers to drive periodic flow through a thin slot in the wall, with amplitudes as high as $0.10U$. This system was used in subsequent experiments as reported by Bake, Kachanov & Fernholz (1996) and Bake, Fernholz & Kachanov (2000).

Using this disturbance-generation concept, a forced perturbation at a single frequency effectively excites the TS waves that are the focus of this study. To do so, periodic suction and blowing through a thin slot in the plate at $x_{TS} = 190$ mm is achieved using an array of loudspeakers. Six loudspeakers are connected to the slot through 40 plastic tubes spanning the width of the slot. A signal generator produces the sine-wave input that is amplified to drive the loudspeakers, which have impedances of 8 Ω and are rated at 100 W. The specific disturbance-generating system in this work has been used in previous experiments, most recently including those by Fransson *et al.* (2005*a*) and Shahinfar *et al.* (2013).

A few different configurations are tested, but the primary results reported here are limited to a test speed of $U_\infty = 12$ m s^{-1} with a forcing frequency $f = 152$ Hz. The non-dimensional frequency is then $F = 2\pi f \nu \times 10^6/U_\infty^2 = 100$. In the context of neutral stability of the zero-pressure-gradient boundary layer, this arrangement of roughness and forcing is depicted in figure 3. The location of the disturbance slot in terms of $R = \sqrt{Re_x}$ is shown as the solid vertical line. Periodic forcing in the boundary layer can also excite stable disturbances (Saric 2007), and a relaxation distance of $10\delta_{99}$ is marked as the vertical dashed line. The streamwise extent of the two roughness types tested is represented by horizontal lines. Taken together, this figure shows that TS waves are excited a short distance upstream of the first neutral stability point so that their initial decay is minimal. Shortly after these disturbances begin to grow, the flow encounters the surface roughness pattern intended to modulate the mean flow and attenuate TS-wave amplification. Finally, the shorter roughness field ($L = 250$ mm) ends a short distance upstream of the second neutral stability point, x_{II}, unlike the longer field with $L = 480$ mm. These parameters are chosen to study the effect of surface modulation on growth rates of TS waves.

A nominally two-dimensional disturbance (i.e. spanwise invariant) is forced using a source which is finite in z and driven by an array of loudspeakers. Velocity-profile measurements at many spanwise locations separated by spanwise steps of $\Delta z = 1$ mm indicate that the mean flow and TS-wave amplitude are sufficiently uniform across the span of the measurement region. The velocity contours of figure 4 illustrate the spanwise-invariance of the flow upstream of the roughness field. Iso-velocity contours of the mean flow in increments of $0.1U_\infty$ are plotted in figure 4(*a*), together with the spanwise-average velocity profile. Additionally, contours of the fluctuation velocity in the TS-forcing band display a similar degree of uniformity in figure 4(*b*). The

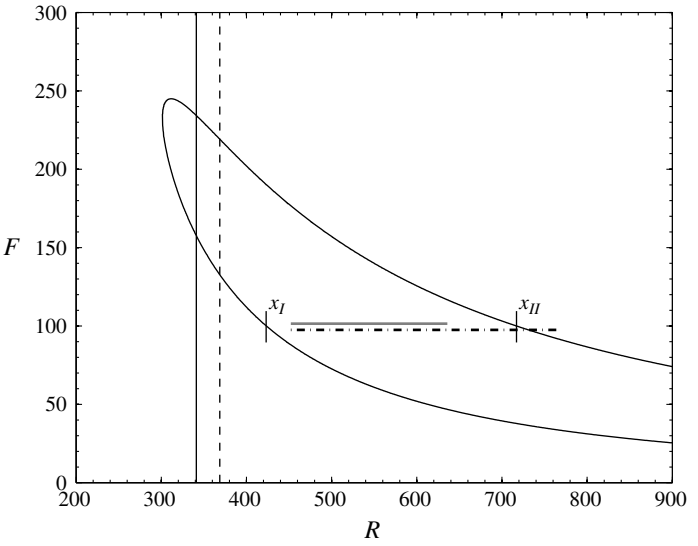

FIGURE 3. Neutral stability curve for zero-pressure-gradient boundary layer. The streamwise extent of the roughness pattern is plotted at the non-dimensional forcing frequency $F = 100$ for [1|λ|250] mm roughness (——) and [1|15|480] mm roughness (-·-·-). The location of the disturbance source is represented by the solid vertical line. The dashed vertical line is $10\delta_{99}$ downstream.

spanwise-averaged TS-wave amplitude profile follows the theoretical shape with a high inner peak and smaller outer peak near $y/\delta = 5$. As the amplitude of the forced TS waves does not significantly vary across the span, reference measurements are made at a single spanwise location.

The amplitude of the TS waves is adjusted by varying the loudspeaker input voltage, V. Although a useful measure for repeating measurements, loudspeaker voltage is of little practical use. Rather, the TS-wave amplitude measured at x_I or x_{II} are more appropriate metrics. Herbert (1988) notes that a local maximum amplitude of 1 % (streamwise root-mean-square (r.m.s.) fluctuation) separates TS waves that decay from those that foster fundamental secondary instabilities and three-dimensionality. Conversely, resonant interaction among fundamental two-dimensional waves and oblique subharmonic waves is observed at amplitudes less than $0.1U$ by Borodulin, Kachanov & Koptsev (2002*b*). In the present experiments, the TS-wave amplitude is computed from frequency-band integration of u' in the range $f_{TS} \pm \Delta f$, with $2\Delta f = 5$ Hz. That is, the power spectra of u' are computed and normalized according to Parseval's theorem (Press *et al.* 2007). The energy associated with the TS wave is then

$$E_{TS}(x, y, z) = \int_{f_{TS}-\Delta f}^{f_{TS}+\Delta f} \mathrm{PSD}(u')\mathrm{d}f. \tag{3.1}$$

The normalized TS-wave amplitude is computed as follows, recognizing that for a sinusoidal signal, the amplitude and the r.m.s. are related by a factor of $\sqrt{2}$,

$$A_{TS}(x, y, z) = \frac{\sqrt{2E_{TS}(x, y, z)}}{U_\infty}. \tag{3.2}$$

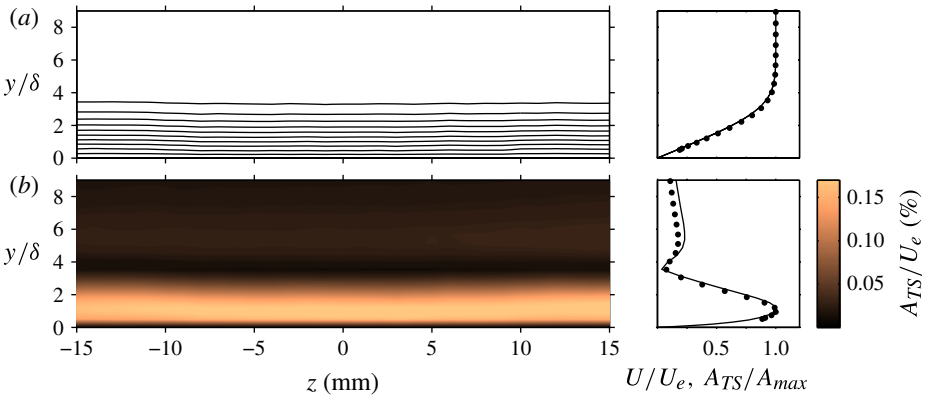

FIGURE 4. (Colour online) A spanwise slice of the boundary layer is measured at $x = 275$ mm ($R = 469$), with $U_\infty = 12$ m s^{-1}, $F = 100$. This is 84 mm downstream of the disturbance slot and 25 mm upstream of the roughness elements. (*a*) Contours of the steady velocity (left) and mean velocity profile (right). (*b*) Contours of TS-wave amplitude (left) and spanwise-mean disturbance profile (right). Points in profiles are measured data. The solid line is the theoretical profile of a two-dimensional TS wave in a Blasius boundary layer at the conditions of the experiment.

Since the shape of the TS-wave amplitude profiles is modified when the mean flow is distorted (Fransson *et al.* 2005*a*), the maxima in y often used as the amplitude in the streamwise direction may underestimate the strength of the TS wave. As such, integrating the profiles in the wall-normal direction using the Blasius coordinate $\eta = y/\delta$ results in a more representative value of the amplitude. Furthermore, the profiles are also integrated in the spanwise direction to account for variations due to mean-flow modulation and secondary instability, using the dimensionless coordinate $\zeta = z/\lambda$. This integrated TS-wave amplitude is then

$$A_{TS}^{int}(x) = \int_{-1/2}^{1/2} \int_{0}^{\eta=9} A_{TS}(x, y, z) \mathrm{d}\eta \mathrm{d}\zeta . \tag{3.3}$$

Using this definition of TS-wave amplitude, reference measurements are made over a smooth plate. In doing so, the data-acquisition system is phase triggered using the loudspeaker input signal. At every point in space, four sets of 3 s long measurements are sampled at 5 kHz and the TS-wave amplitude is computed using a frequency-domain average of the sets. The TS-wave amplitudes measured at x_I and x_{II} are tabulated with the loudspeaker forcing voltages for reference in table 2. For comparison with earlier literature, r.m.s. amplitudes are also given, though the discussion in the present work is limited largely to integrated amplitudes. Disturbance amplification is computed as $\ln(A_{TS}^{int}/A_0)$, where A_0 is the integrated amplitude of the disturbance at the first streamwise measurement position. For several forcing amplitudes, the resulting amplification curves of figure 5 depart from linearity at larger values. Up to a branch I amplitude of $A_{TS}^{int,I} = 1.1\,\%$, these growth rates are nearly coincident and, thus, do not depend on the forcing amplitude. For values above this, the TS waves become three-dimensional and the growth curves do not collapse on those of the two-dimensional TS waves. For this divisive test cast, the corresponding branch II amplitude is $A_{TS}^{int,II} = 3.7\,\%$ and the local maximum value is

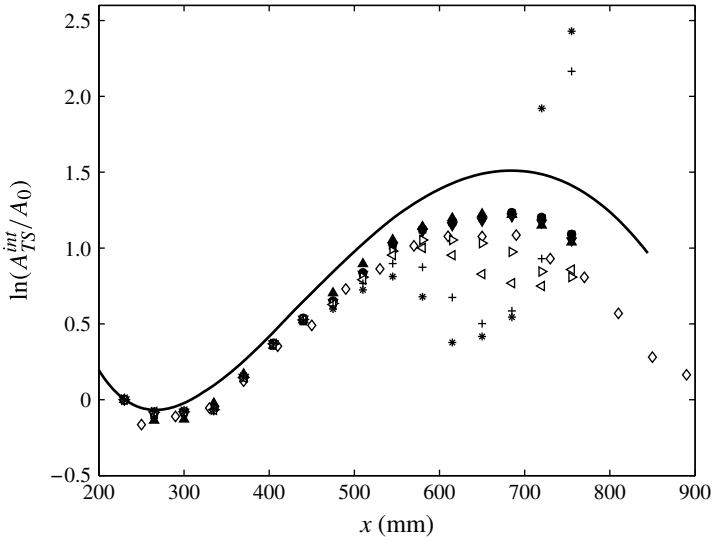

FIGURE 5. TS-wave growth curves measured using several forcing amplitudes at $U_\infty = 12$ m s^{-1}, $F = 100$. The initial amplitudes are $A_{TS}^{int,I} = 0.18\,\%$ (■), $0.38\,\%$ (●), $0.48\,\%$ (▲), $0.78\,\%$ (▼), $1.11\,\%$ (◇), $1.57\,\%$ (▷), $1.97\,\%$ (◁), $2.59\,\%$ (+), $3.20\,\%$ (∗). The solid line results from linear stability theory calculations of two-dimensional TS waves in a zero-pressure-gradient boundary layer at $U_\infty = 12$ m s^{-1}, $F = 100$, and is based on the integral measure of TS-wave amplitude.

1.41 %. Removing a factor of $\sqrt{2}$ produces the expected equivalent r.m.s. value of 1 %. For comparison, the growth curve for a two-dimensional TS wave with $F = 100$ is also included in figure 5. This growth curve is computed using linear stability theory for a zero-pressure-gradient boundary layer at $U_\infty = 12$ m s^{-1}, and is shifted in x by the virtual leading edge location. It is further noted that while this represents a strictly two-dimensional TS wave, the measured disturbances have a small degree of three-dimensionality. This theoretical curve is characterized by a slightly higher amplification ratio. The sensitivity of TS waves to small pressure gradients near branch I is well-known, and the initial development of the mean flow observed in the upstream region of figure 1(*a*) deviates significantly from the theoretical assumptions. As such, the discrepancy between theory and the present experiments is not unexpected. For the purpose of a relative study of TS-wave development, this set of basic disturbances is suitable.

To examine the interaction between linearly growing TS waves and modulated mean flow due to the surface roughness pattern, the forcing amplitude is set such that the maximum r.m.s. at x_{II} is 0.53 %, corresponding to the $A_{TS}^{int,I} = 0.48\,\%$ case of figure 5. This produces well-resolved amplitude profiles while avoiding the complications of secondary instabilities in the reference case. The effect of three-dimensionality of the TS waves is also tested using the larger forcing amplitudes of figure 5.

4. Roughness-induced effects

The present work is concerned with development of TS waves in modulated flows, their role in the transition process and the potential for delaying transition. Due to the novel nature of the surface roughness field, it is worthwhile to consider first

V (mV)	$A_{TS}^{int,I}/U_\infty$ (%)	$A_{TS}^{rms,I}/U_\infty$ (%)	$A_{TS}^{int,II}/U_\infty$ (%)	$A_{TS}^{rms,II}/U_\infty$ (%)
50	0.182	0.040	0.675	0.183
100	0.384	0.081	1.437	0.369
150	0.482	0.113	1.857	0.531
200	0.775	0.165	2.807	0.737
300	1.113	0.223	3.677	1.000
400	1.569	0.334	4.501	1.416
500	1.971	0.421	4.604	1.570
650	2.591	0.553	4.975	1.271
800	3.195	0.687	5.940	1.808

TABLE 2. Comparison of normalized TS-wave amplitudes measured at the neutral stability points. Integrated amplitudes are computed using (3.3). A_{TS}^{rms} values are maxima of $A_{TS}(y)/\sqrt{2}$ profiles, and are approximately equivalent to the $u'_{rms,max}$ measure common in the literature.

how the mean flow is deformed. Changes to the evolution of TS waves may be better understood in the context of mean-flow modifications. The results return to the motivating phenomenon: altering the laminar-to-turbulent transition location via regularly patterned surface features. The role of unsteady disturbance characteristics is further examined by adding moderate deviations to the forcing frequency. Finally, the results conclude with a comparison of estimated skin-friction drag due to roughness and boundary-layer transition.

4.1. *Mean-flow modification*

As discussed previously, the surface roughness pattern is intended to introduce spanwise shear to the mean flow while minimally affecting the boundary layer otherwise. It is known that high-amplitude streaks in the far wakes of roughness elements are subject to secondary instabilities, and that for large Re_k, instability in the near wake amplifies unsteady fluctuations that rapidly incite transition (Ergin & White 2006). Thus, it is important to investigate the flow topology over the roughness pattern and in its wake. A common difficulty in boundary-layer measurements with hot-wire probes is location of the wall in traverse coordinates. To avoid erroneous measurements of the quantity resulting from roughness-deformed velocity profiles (White & Ergin 2004), wall-location measurements are made before the roughness is installed. The accurately known roughness shape and smooth-wall locations are incorporated into the probe-traversing algorithm to allow measurement of boundary-layer velocity profiles on the surface and in the near wakes of the roughness field. To ensure probe safety, the probe is never moved closer to the surface than 0.25 mm.

Measurements of the mean flow in the presence of the surface roughness are made concurrently with moderate-amplitude TS waves. The TS-wave amplitudes are small enough that they do not affect the mean flow, but decay downstream of branch II. To assess the character of the flow within the boundary layer, contours of the shape factor H highlight deviations from the basic state of the mean flow. Considering the flow measured with three different roughness wavelengths in figure 6, a few key characteristics may be discerned. In this figure, outlines of single roughness elements are shown for reference, though the plots are stretched significantly in the z direction

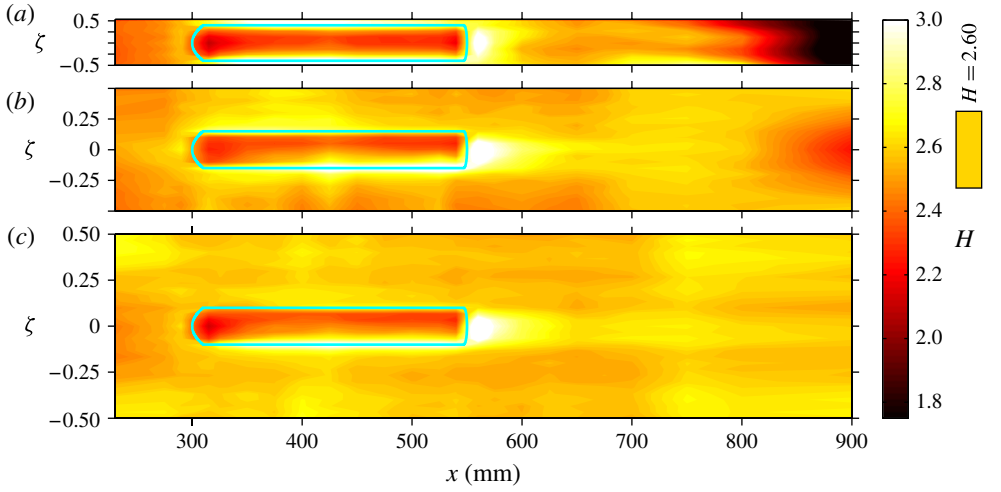

FIGURE 6. (Colour online) Contours of boundary-layer shape factor, H. The flow conditions are $U_\infty = 12$ m s^{-1}, $F = 100$ with (*a*) [1|7.5|250] mm roughness, (*b*) [1|20|250] mm roughness, and (*c*) [1|30|250] mm roughness.

for clarity. As such, the leading and trailing edges of the roughness appear more blunt than their physical counterparts. Recalling that the mean basic-state H value is 2.60, it is observed that flow over the surface of the roughness produces lower values of H, particularly near the leading edges of the roughness. This indicates that rather than a simple vertical displacement, the boundary layer is squeezed as the flow climbs onto the roughness. This is manifested as an accelerated velocity profile. Conversely, the trailing edges of the roughness are characterized by profiles which appear decelerated, as the roughness surface drops away under the previously accelerated profiles. The flow appears to recover to a large degree by $x = 600$ mm, or $50k$ downstream of the trailing edge. In figure 6(*a*), the roughness pattern with the shortest wavelength is shown: $\lambda = 7.5$ mm, or $\lambda/s = 1.25$. In this case, flow in between the roughness is restricted by the small interstitial gaps, as evident in the high-H profiles on the flanks of the roughness. For this configuration with low-amplitude TS-wave forcing, the flow is comparatively unstable. The drop in H to approximately 1.8, which is closer to the value of 1.4 expected of developed turbulent velocity profiles, indicates transition near $x = 900$ mm.

Lateral asymmetry of H contours in figure 6 is observed on the long edges of the roughness, particularly near the trailing edges. This appears to result from misalignment between the flow direction and roughness axis. Detailed flow measurements in an empty test section (Lindgren & Johansson 2002) show that flow angularity is 0.1° or less in the region of the test section relevant to these measurements. Roughness elements are aligned perpendicularly with the plate leading edge. The observed spanwise misalignment is small: less than 0.6 mm in the spanwise direction over the $L = 250$ mm roughness length, as the probe never collided with the roughness despite close approaches on both sides of roughness surface. In the case of the shape-factor measurements of figure 6 in which the boundary-layer wall locations are shifted by the roughness shape, a displacement of the roughness 0.2 mm in the positive ζ direction can produce a wall-location error sufficient to explain the

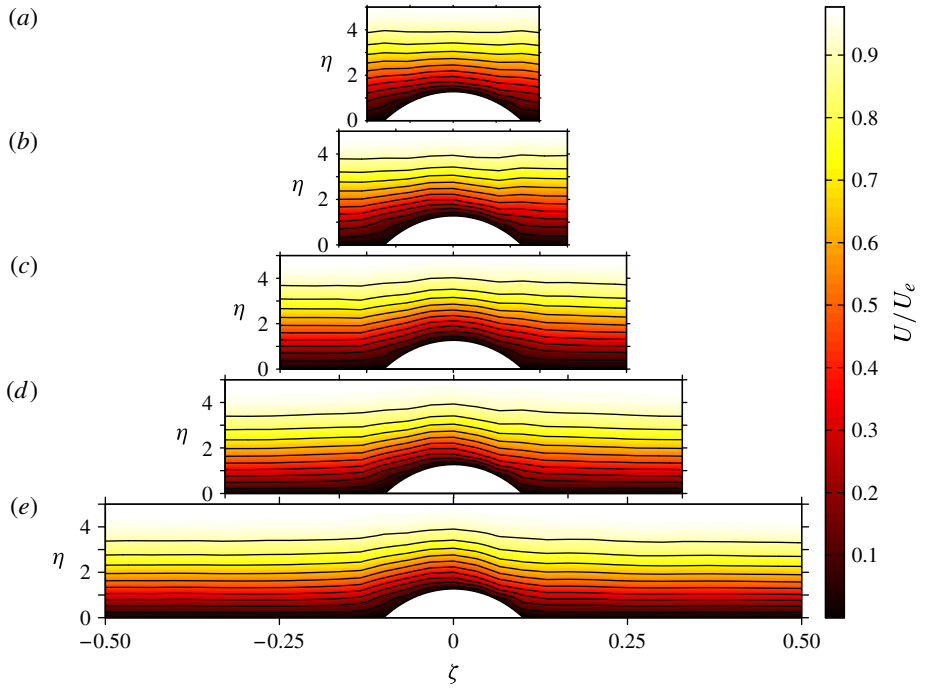

FIGURE 7. (Colour online) Contours of the mean velocity at $U_\infty = 12$ m s^{-1}, $F = 100$ with $k = 1$ mm, $L = 250$ mm roughness with wavelength $\lambda =$ (*a*) 7.5 mm, (*b*) 10 mm, (*c*) 15 mm, (*d*) 20 mm, (*e*) 30 mm. Measurements are made at $x = 500$ mm.

asymmetry. That it, these measurements indicate that the angle between the flow direction and the roughness axis is approximately 0.05°.

Examining the structure of the flow in streamwise planes confirms the shape-factor-based observations. For most of the experimental configurations, y–z planes are measured at many streamwise locations and a collection of such planes measured at $x = 500$ mm is shown in figure 7. The mean streamwise velocity is displayed as iso-velocity lines in increments of $0.1U_\infty$ and also as colour contours. The spanwise extent of each plot is $-0.5 \leqslant \zeta \leqslant 0.5$, and the plots are scaled to the same physical dimensions. This streamwise location is $0.8L$ toward the end of the roughness pattern. Flow over the roughness has developed from the disturbances associated with the leading edge of the roughness. The closely spaced contour lines near the peak of the humps indicate that the boundary layer is compressed somewhat in the vertical direction. Rather than a direct modulation of the boundary layer, the flow appears somewhat elastic in the sense that the presence of the hump is not felt as strongly high in the boundary layer. Indeed, in figure 7(*a*), the top-most contour line is approximately flat. Conversely, for the longest wavelength in figure 7(*e*), there are large outboard regions of apparently unperturbed flow. As the intent is to produce spanwise shear in the mean flow, these two cases form brackets around the optimal λ/s in a flow deformation sense.

To examine the wake regions in greater detail, the [1|15|250] mm pattern is considered and a finely resolved x–z plane of velocity measurements is made at $\eta = 1.2$, or $U/U_\infty = 0.4$ for Blasius flow. This so-called plane is not parallel to the plate as it follows the boundary-layer growth. The contours of figure 8(*a*) span

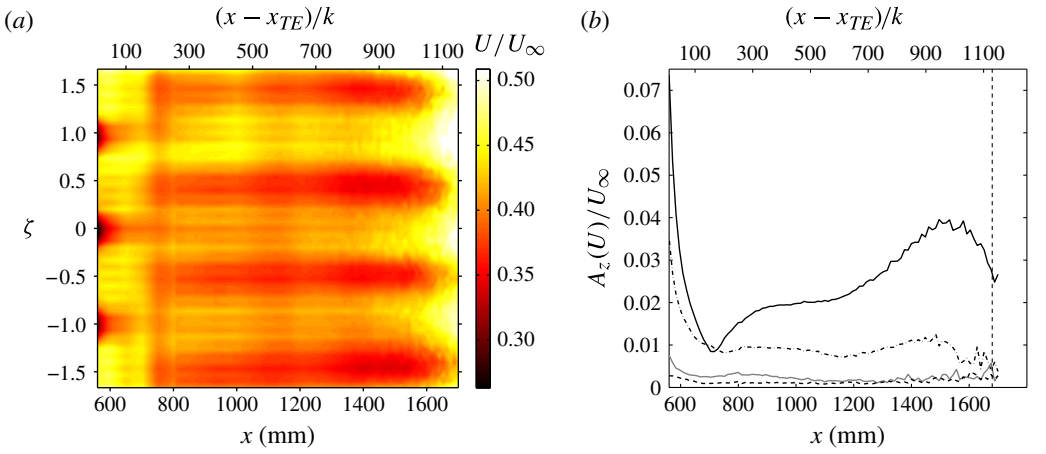

FIGURE 8. (Colour online) Boundary-layer measurements at height $\eta = 1.2$, with $U_\infty = 12$ m s^{-1}, $F = 100$. The trailing edge of the [1|15|250] mm roughness is at $x_{TE} = 550$ mm. (*a*) Contours of mean flow, and (*b*) amplitudes of spanwise components of mean flow: λ (——), $\lambda/2$ (·····), $\lambda/3$ (——, grey), and $\lambda/4$ (- - -). The onset of turbulent flow, defined as 50 % intermittency, is marked with a vertical dashed line.

three roughness wavelengths with roughness centrelines at $\zeta = -1$, 0, 1, and extend from the near wake of the roughness to the beginning of the transitional region. At the left-hand edge of this plot, the decelerated regions in the near wakes of the roughness are visible. As the flow progresses downstream, lower-speed regions evolve between the roughness elements. Although the far wakes do not develop strong high-speed streaks, this pattern of mean-flow modulation is not unlike that of the roughness-induced disturbances driven by streamwise vorticity. In this case, the magnitude of the mean-flow variation is relatively small.

A spectral analysis of the velocity contours of figure 8(*a*) is presented in figure 8(*b*). Briefly, the steady disturbances $U'(x, y, z) = U(x, y, z) - U^z(x, y)$ are computed at each x location where U^z is the spanwise average of U. Spanwise spatial power spectra $\mathrm{PSD}_z(U^z)$ are estimated using squares of the Fourier coefficients of U' and normalized such that the sum of the λ-mode and its harmonics is equal to the square of the spanwise r.m.s. of U'. The plotted amplitudes are then $A_z = \sqrt{2\mathrm{PSD}_z}$. Streamwise development of the mean-flow disturbance with λ and its first three spanwise harmonics is computed and shows that all modes except the fundamental decay rapidly. The λ-mode, however, initially decays sharply as the flow recovers from the near wake before growing as the areas of low-speed flow develop downstream of the interstitial spaces. A region of increased growth is observed beginning near $x = 1200$ mm. As the boundary layer becomes turbulent, increased mixing destroys spatial periodicity in the mean flow and the λ-mode decays. The streaks in the mean flow are relatively weak at less than 10 % of U_∞, and secondary instability of the streaks is unlikely. That is, transition appears to result from controlled excitation of TS waves as intended.

4.2. *TS-wave growth and transition*

A study of how low-amplitude TS waves develop is useful as disturbance growth in the reference case remains two-dimensional throughout the region of interest.

Furthermore, relative growth rates are largely unchanged for small initial amplitudes (as in figure 5), facilitating a quantitative comparison. The reference case is labelled $A_{TS}^{int,I} = 0.48\,\%$ in figure 5. The corresponding branch II maximum r.m.s. is 0.53 % of U_∞, which is approximately half that needed for secondary instability. The same forcing amplitude is applied to boundary layers in which the patterned surface roughness is deployed. Streamwise fields of TS-wave amplitude show that two-dimensionality of the TS waves is disrupted by the modified mean flow, as in figure 9(*a*). In these contour plots, which represent the same location and conditions as figure 7, the solid lines are constant TS-wave amplitude. The colour contours are also mapped to TS-wave amplitude. For reference, selected TS-wave profiles in figure 9 illustrate how the shape of three-dimensional waves differ from the two-dimensional reference case.

The closely spaced roughness pattern of figure 9(*a*-i) promotes TS-wave growth on the peak of the roughness and on the flanks, as indicated by the three high-amplitude spots in the contour levels. Comparing profiles of the TS-wave amplitude with the reference case, the maxima are approximately twice as high in the modulated case. As the wavelength is increased and the mean flow is deformed less harshly, the effect on TS-wave amplitude becomes favourable. The same three local maxima are observed, but those on the flanks of the roughness are less pronounced than in the short-wavelength case. Similarly, the portion of the TS wave travelling over the ridges of the roughness become less intense as the flow in the interstitial spaces is less constrained by neighbouring roughness. Likewise, the amplitude profiles show similar reductions in intensity relative to the reference case. In figure 9(*a*-iv), the TS-wave amplitude profile on the roughness peak is approximately the same as the reference case, but displaced vertically. The amplitudes are reduced elsewhere. For $\lambda < 15$ mm and $\lambda = 30$ mm and, TS waves travelling over roughness peaks are amplified to a greater degree than in the reference case. However, as roughness wavelength (or opening width) is increased, TS-wave amplitudes are still slightly reduced in the open spaces below reference-case values. In the widest-opening case, increased disturbance growth and less-effective control compared with shorter wavelengths is related to local amplification of TS waves over the roughness surface.

Moving downstream to $x = 700$ mm, which is past x_{II} and 150 mm downstream of the roughness pattern, the lingering influence of the roughness on TS-wave growth is illustrated by figure 9(*b*). When the roughness is closely spaced as in figure 9(*b*-i), its influence is detrimental to flow stability. The flow is becoming transitional and the TS-wave amplitudes are several times that of the reference case. The wider spacing of figure 9(*b*-ii) is a marked improvement. The unsteady disturbances are slightly larger than those of the unmodified boundary layer. The centreline TS-wave profile follows a distinctive M-shape which has been observed previously in modulated boundary layers (Fransson *et al.* 2005*a*; Shahinfar *et al.* 2013). Following this trend, wider spacing of the roughness pattern produces lower TS-wave amplitudes at this streamwise location until $\lambda = 30$ mm in figure 9(*b*-v). In this case, larger disturbances are observed in the outboard regions, apparently due to disturbance growth in the wide interstitial spaces. Of particular interest is the distribution of amplitudes when $\lambda = 20$ mm in figure 9(*b*-iv). A typical M-shaped profile is observed, but perhaps more telling is the spanwise symmetry of the disturbances. This indicates an order to the flow which is absent in the other cases.

The evolution of disturbances at the forcing frequency is quantified via integration in y–z planes as described previously. Although this procedure may be reductive of local instability growth, the summarized growth curves of figure 10 illustrate

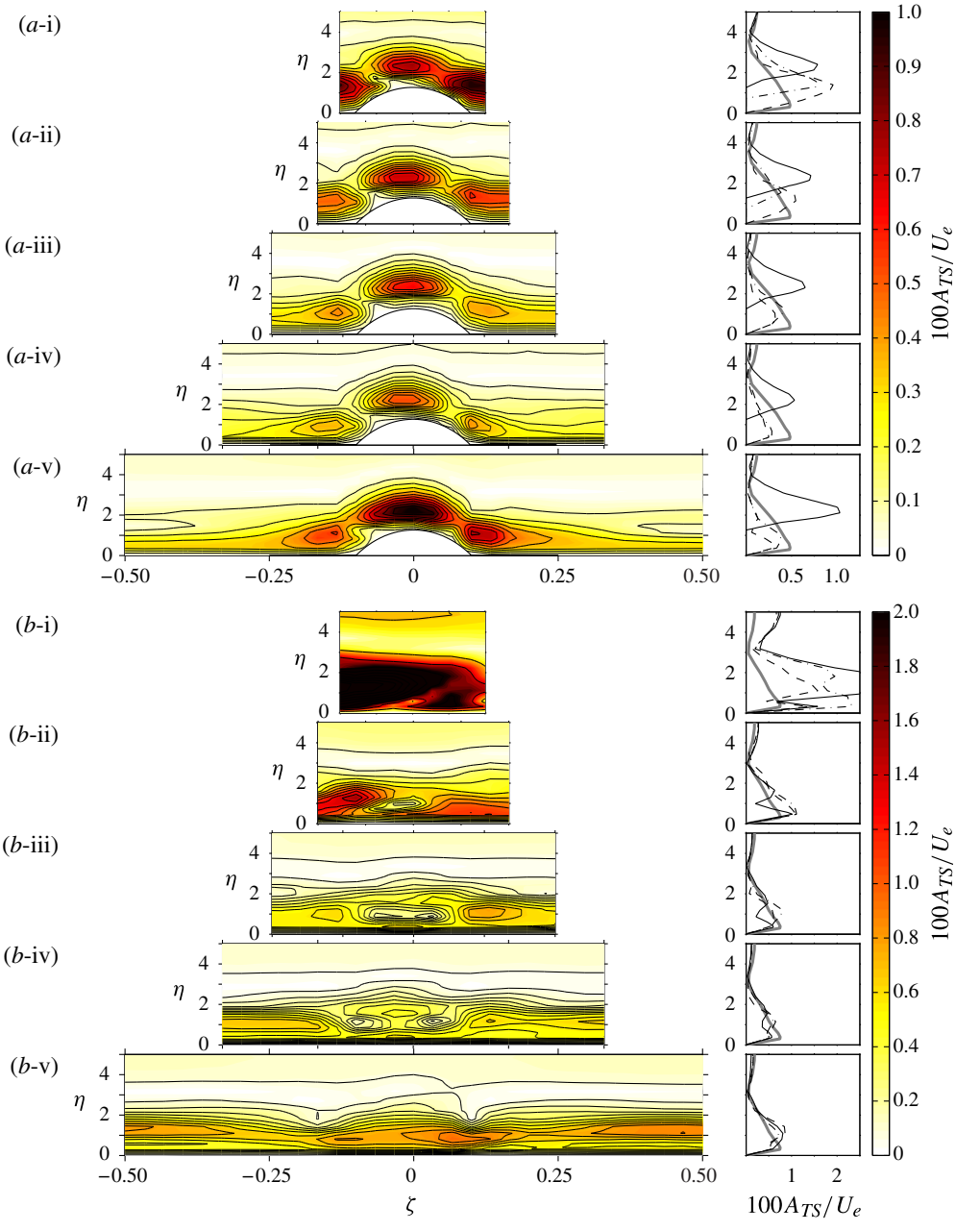

FIGURE 9. (Colour online) Contours of TS-wave amplitude (left) and TS-wave profiles (right) at $U_\infty = 12$ m s^{-1}, $F = 100$ with $k = 1$ mm, $L = 250$ mm roughness. (*a*) Measurements at $x = 500$ mm and (*b*) measurements at $x = 700$ mm. Wavelengths are $\lambda = 7.5$, 10, 15, 20, and 30 mm in (i)–(v) respectively. TS-wave profiles are plotted for $\zeta = 0$ (——), $\zeta = 0.25$ (·····) and $\zeta = 0.5$ (- - -). The reference case TS-wave profiles are plotted as thick solid lines.

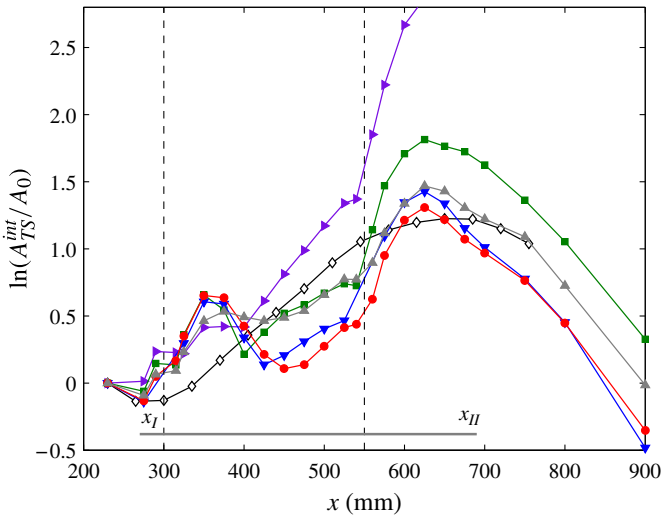

FIGURE 10. (Colour online) Relative amplification of TS waves in the reference case (◇), and with $L = 250$ mm roughness, $\lambda = 7.5$ mm (▶), $\lambda = 10$ mm (■), $\lambda = 15$ mm (▼), $\lambda = 20$ mm (●), $\lambda = 30$ mm (▲). The flow is $U_\infty = 12$ m s^{-1} with $F = 100$ forcing ($A_{TS}^{int,I} = 0.48\,\%$). Vertical dashed lines denote the streamwise extent of the roughness field; horizontal line marks branch I and branch II locations, relative to the virtual leading edge location at $x_{vle} = 44.5$ mm.

the leading effects of the roughness field. The growth curve associated with the two-dimensional reference case is included and follows the expected shape. All such curves are normalized using the initial amplitude rather than that measured at branch I. The leading and trailing edges of the roughness field are marked with vertical dashed lines. In all cases with artificial roughness, the leading edge produces an initial amplification of the forced disturbances. After a short relaxation distance, the disturbances begin to decay before growing at a reduced rate compared with the reference case. As indicated by the TS-amplitude contours of figures figure 9(*a*-i) and 9(*b*-i), disturbance growth in the $\lambda = 7.5$ mm case increases sharply. The other cases, however, demonstrate significant attenuation of TS-wave amplitude at the trailing edge of the roughness field. This effect is overshadowed by sharp disturbance growth in the near wake of the roughness, and the amplitudes at x_{II} are larger in all roughness-modified cases except $\lambda = 15$ and 20 mm.

The additional disturbance growth at the leading and trailing edges of the roughness field may be due to interaction of roughness-induced vorticity and either free-stream acoustic or vortical disturbances. For example, Ruban (1984) found that acoustically driven disturbances can interact with a hump-shaped roughness element, and predicted the growth of TS waves aft of the hump. Acoustic receptivity resulting from a wall bump was computed by Nayfeh & Ashour (1994), who treated disturbed flow as the sum of a Stokes waves (the acoustic disturbance) and a travelling wave (TS wave). The largest disturbance growth was observed when the hump was placed just downstream of branch I of the neutral stability curve, as in the present experiments. Ruban, Duck & Zhikharev (1996) describe a mechanism of TS-wave excitation in which free-stream vorticity interacts with roughness-induced disturbances penetrating the upper regions of the boundary layer. However, it is noted that 'for boundary-layer

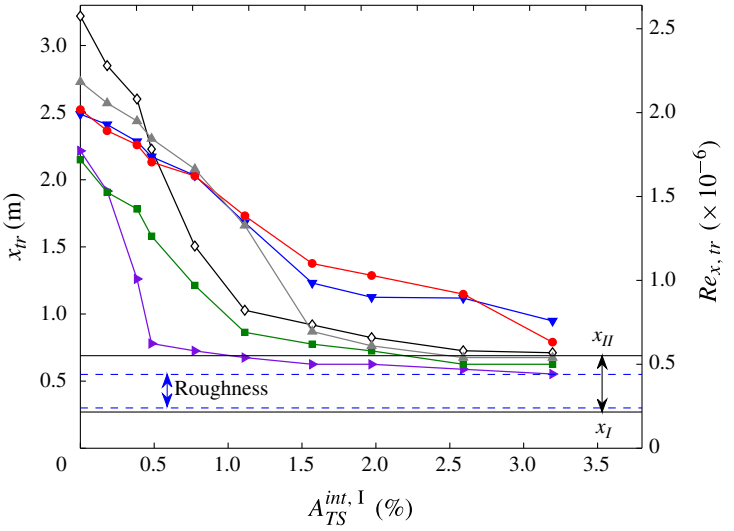

FIGURE 11. (Colour online) Transition location as a function of initial forcing amplitude for the reference case (◊), and with $L = 250$ mm, $\lambda = 7.5$ mm (►), $\lambda = 10$ mm (■), $\lambda = 15$ mm (▼), $\lambda = 20$ mm (●), $\lambda = 30$ mm (▲). The flow is $U_\infty = 12$ m s^{-1} with $F = 100$. Solid horizontal lines mark the TS-growth region, and dashed lines mark the streamwise extent of the roughness field.

flows, the resonance between external disturbances and internal instability waves supposes coincidence not only of frequencies, but also of wavenumbers'. The simulations of Wu (2001) demonstrate that receptivity to vortical disturbances is larger than previously thought, yet a less efficient generator of TS waves than acoustic disturbances. Thus, acoustic disturbances in the free stream or emanating from the disturbance slot and interacting with the vorticity shed by the roughness field may account for the brief regions of disturbance amplification observed in figure 10. Additionally, as found by Ustinov (1995), a planar TS wave impinging on an isolated roughness element scatters disturbances at the fundamental frequency in a manner similar to that of a turbulent wedge. Evolution of disturbances in these regions may involve additional receptivity and scattering of oblique waves.

A detailed study of the combined roles of the roughness field and TS-wave forcing on transition is completed by varying both the roughness wavelength and the forcing amplitude, using the roughness configurations and forcing amplitudes established in tables 1 and 2, respectively. Transition is detected using the intermittency estimation technique of Fransson, Matsubara & Alfredsson (2005*b*). Briefly, velocity time records are subjected to a high-pass filter with cut-off frequency $f_c = U_\infty/(5\delta_{99})$ and a detector function discriminates turbulent bursts in the filtered data. Sensing thresholds are varied and an estimate of the intermittency function γ is extrapolated. As transition in this scenario is typically accompanied by a protracted intermittency region, the onset of transition is taken as the location when $\gamma = 0.5$. The necessity of more finely resolved measurements in x precludes the possibility of measuring full y–z planes, rather, roughness-centreline velocity profiles are measured. The transition location via γ is evaluated at $y = \delta^*$. Because the wall-normal distribution of γ does not vary too strongly in the lower region of the boundary layer, the additional uncertainty in

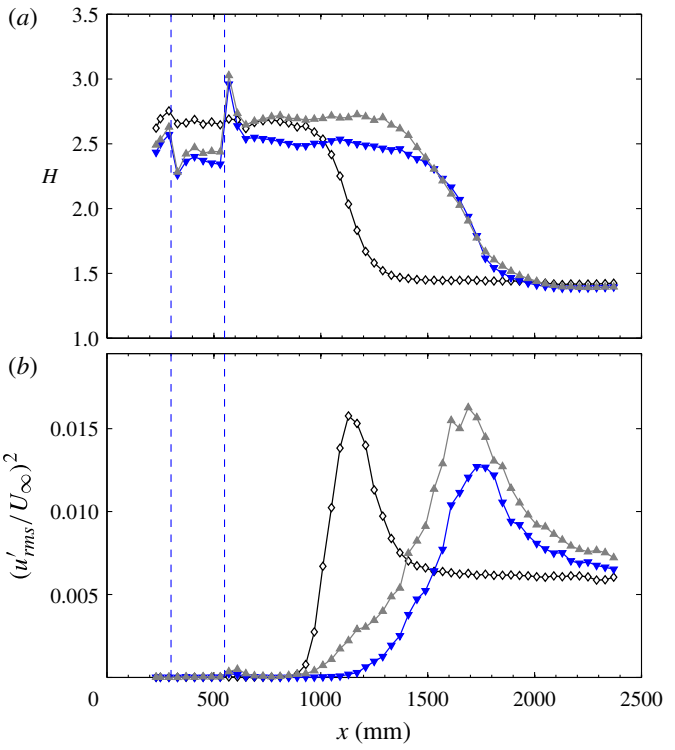

FIGURE 12. (Colour online) (*a*) Shape factors and (*b*) streamwise fluctuation energy at $y = \delta^*$. The test condition is $U_\infty = 12$ m s^{-1} with $F = 100$, $A_{TS}^{int,I} = 1.1\,\%$ forcing. Two-dimensional reference case measurements (◇) are compared with $L = 250$ mm roughness with $\lambda = 15$ mm (▼) and $\lambda = 30$ mm (▲). Vertical dashed lines mark the streamwise extent of the roughness.

transition location is minimal. Results of the transition measurements are shown in figure 11, in which transition location is plotted as a function of TS-wave amplitude for different roughness wavelengths.

Several important conclusions may be drawn from these data. First is the observation that at low amplitudes of unsteady forcing and in the unforced case the roughness accelerates transition in all studied configurations. At these conditions ($A_{TS}^{int,I} < 0.5\,\%$), the transition location moves forward with decreasing λ, and $Re_{x,tr}$ remains above 1.5×10^6 for all but the $\lambda = 7.5$ mm case. As expected, transition moves forward universally with increasing forcing amplitude. It is, however, the relative change in transition location with λ at fixed forcing amplitude which is of interest. For small-amplitude forcing, the roughness is detrimental, in that it advances transition compared with the reference case. For moderate forcing amplitudes that exceed the secondary instability threshold, transition is delayed in some cases compared with the reference case. Specifically, $\lambda \geqslant 15$ mm produces delayed transition. At higher amplitudes, the $\lambda = 15$ and 20 mm roughness fields are the only tested wavelengths effective in delaying transition. This transition delay is considerable: in one case, the extent of laminar flow is 70 % greater when the roughness pattern is present.

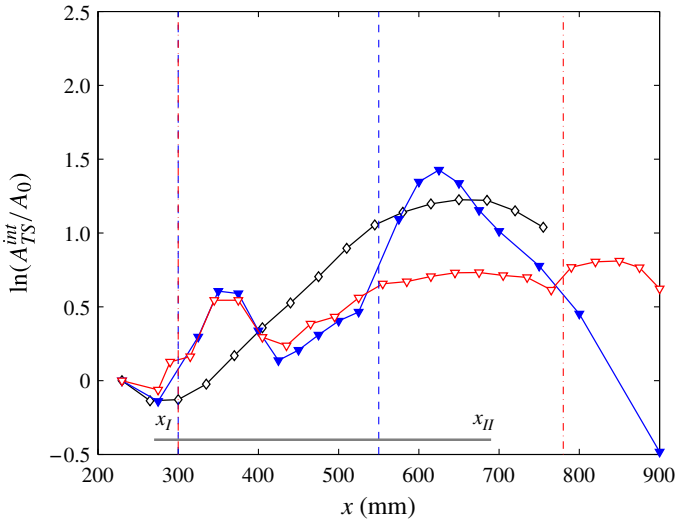

FIGURE 13. (Colour online) Relative amplification of TS waves in the reference case (◇), with [1|15|250] mm (▼), and [1|15|480] mm roughness (▽). The flow is $U_\infty = 12$ m s^{-1} with $F = 100$ forcing ($A_{TS}^{int,I} = 0.48\,\%$). Vertical dashed lines denote the streamwise extent of the roughness fields $L = 250$ mm (- - -) and $L = 480$ mm (-·-·-). Horizontal line marks x_I and x_{II}, relative to x_{vle}.

This most-successful configuration employs $\lambda = 15$ mm roughness with $A_{TS}^{int,I} = 1.1\,\%$ forcing, and is examined in detail with measured velocity profiles. The boundary-layer shape factors resulting from these profiles are plotted in figure 12(*a*). Acceleration of the flow onto the roughness surface is evident in the lowered H values, followed by deceleration in the wake. The mean flow recovers, before falling to $H \approx 1.5$ as the boundary layer becomes fully turbulent. Evolution of the streamwise component of the turbulent kinetic energy $(u'_{rms}/U_\infty)^2$ in figure 12(*b*) complements these observations. The onset of transition is accompanied by sharply rising energy which overshoots in the vicinity of $\gamma = 0.5$ before falling to a constant value as the flow becomes fully turbulent. Both the mean and fluctuating components of the hot-wire signal indicate a significant delay in the onset of transition.

Although the goal of transition delay is realized, instability growth associated with the trailing edge of the roughness is an apparent shortcoming. To address this problem, the roughness pattern is extended in the streamwise direction to $L = 480$ mm. This places the trailing edge aft of branch II in the reference case. When compared to measurements using a [1|15|480] roughness pattern, the TS-wave growth curves of figure 13 show a similar development in the upstream region. Whereas the disturbances increased sharply aft of $x = 550$ mm previously, this is avoided by using the longer roughness pattern. At the reference case branch II location, a significant attenuation of the TS-wave amplitude is observed. Finally, a smaller increase in the TS-wave amplitude is observed in the wake of the longer roughness pattern. For low-amplitude forcing, a [1|15|480] roughness pattern is an effective method of controlling the growth of TS waves.

The results of a transition study, however, show that this type of roughness is less effective for transition delay. Although figure 14 does indicate that transition delay is possible for moderate-amplitude TS waves, this extent is somewhat reduced compared

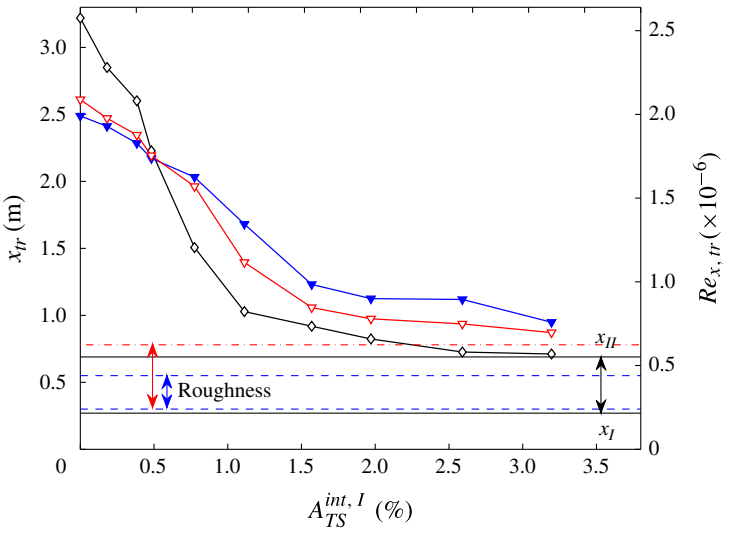

FIGURE 14. (Colour online) Transition location as a function of initial forcing amplitude for the reference case (◊), and [1|15|250] mm roughness (▼), and with [1|15|480] mm roughness (▽). The flow is $U_\infty = 12$ m s^{-1} with $F = 100$. Solid horizontal lines mark the TS-growth region, and dashed lines mark the streamwise extent of the roughness fields: $L = 250$ mm (- - -) and $L = 480$ mm (-·-·-).

with the shorter roughness pattern. One explanation for this is that the Re_x value associated with the wake is increased in this arrangement, and as such, the boundary layer is more susceptible to wake-related disturbances. Similarly, delayed relaxation of the near wake may affect the onset of secondary instabilities leading to transition. The boundary-layer shape factors and fluctuation energy development of figure 15 both confirm the transition delay for the most effective configuration. The [1|15|480] pattern still produces a significant delay in the onset of transition.

4.3. *Forcing frequency effects*

The results of the preceding section are limited to one frequency and free-stream speed while roughness wavelength and streamwise extent are changed. These conditions are deliberately chosen based in part on fixed quantities such as location of the disturbance slot to produce amplified TS waves at the roughness location. As roughness wavelength affects the ability of mean-flow disturbances to attenuate TS-wave growth and delay transition, variation in forcing frequency is also tested to examine its potential role. Keeping speed and roughness location fixed, F is increased from 100 to 110, 120 and 130; this is intended as a modest deviation from the primary test conditions of this work. TS-wave growth curves are measured with $\lambda = 15$ mm roughness and compared with their two-dimensional reference counterparts in figure 16. Because the speed is fixed at $U = 12$ m s^{-1}, the TS-unstable region becomes smaller in streamwise extent and is moved forward with increasing frequency, as noted by the horizontal lines in this figure. Whereas the roughness location is fixed, TS waves experience a longer region of growth before encountering the roughness when the frequency is increased. The result is that interaction with the roughness leading edge amplifies the unsteady disturbances more strongly the further

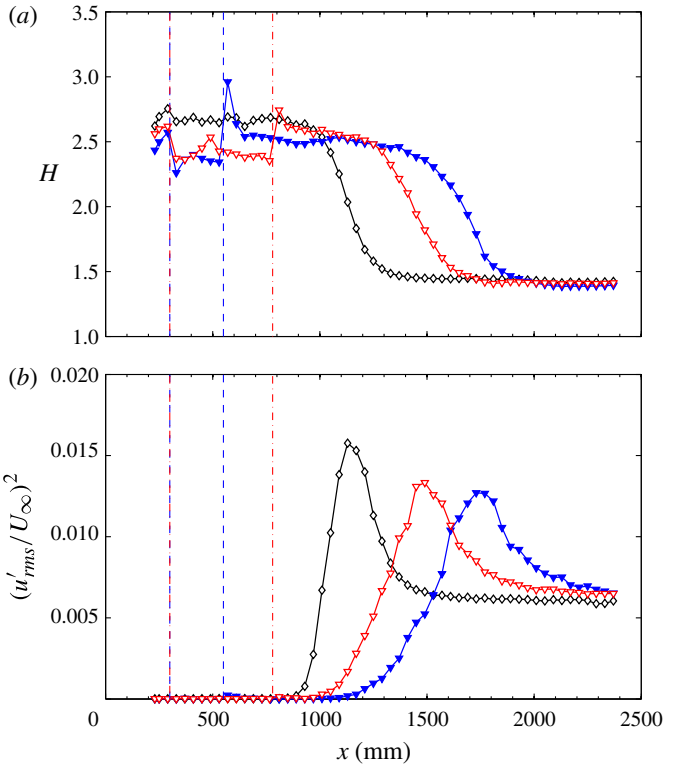

FIGURE 15. (Colour online) (*a*) Shape factors and (*b*) streamwise fluctuation energy at $y = \delta^*$. The test condition is $U_\infty = 12$ m s^{-1} with $F = 100$, $A_{TS}^{int,I} = 1.1\,\%$ forcing. Two-dimensional reference case measurements (◇) are compared with [1|15|250] mm roughness (▼) and [1|15|480] mm roughness (▽). Vertical dashed lines mark the streamwise extent of the roughness fields: $L = 250$ mm (- - -) and $L = 480$ mm (-·-·-).

downstream of x_I the roughness is placed. Conversely, TS-wave interaction with disturbances associated with the roughness wakes is diminished at higher frequency. This is due to comparatively reduced growth rates of TS waves at higher frequency. As a result of these measurements, it is concluded that the roughness extent should cover and exceed the TS-unstable region to maximize attenuation.

Transition induced by low- to moderate-amplitude TS waves at $F = 120$ is summarized in figure 17. The higher-frequency TS waves are less unstable than those of figure 11 and this is reflected in the slightly higher $Re_{x,tr}$ values. Although increasing forcing amplitude gradually moves transition forward, this effect is far less pronounced at lower amplitudes ($A_{TS}^{int,I} < 1.3\,\%$). At higher amplitudes, delayed transition compared with the reference case is observed for roughness with $\lambda > 15$ mm. As with disturbances excited at $F = 100$, the mid-range roughness wavelengths 15–20 mm most effectively maintain laminar flow. The largest difference is that transition downstream of $\lambda = 20$ mm roughness is nearly unaffected by TS-wave forcing at amplitudes up to $A_{TS}^{int,I} = 2.5\,\%$.

These results taken together with those regarding roughness wavelength variation demonstrate that precise tuning of forcing frequency or wavelength is not necessary to delay transition. These characteristics in addition to roughness location and streamwise

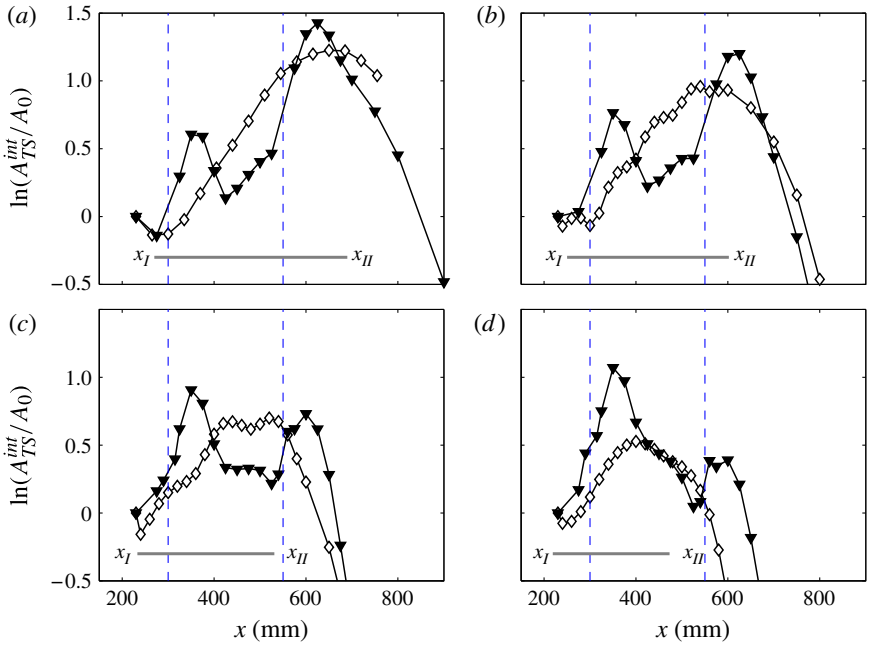

FIGURE 16. (Colour online) TS-wave amplitudes in two-dimensional reference case measurements (◊) compared with [1|15|250] mm roughness (▼), measured at $U_\infty = 12$ m s^{-1}. The dimensionless forcing frequency is (*a*) $F = 100$, (*b*) $F = 110$, (*c*) $F = 120$, (*d*) $F = 130$.

extent can be optimized for TS-wave attenuation or suppression. Undertaking this task will invariably reveal more details of this stabilization mechanism. From a practical viewpoint, these observations bolster the case for further investigation in that the potential for transition delay is tolerant to at least minor variations in flow conditions.

4.4. *Drag analysis*

The results of § 4.2 demonstrate that drag reduction via transition delay may be possible in certain circumstances. However, it must also be shown that artificial surface roughness and its induced disturbances do not impose more drag than they alleviate. Modulation of the mean flow and the additional wetted surface area of the roughness will certainly increase skin-friction drag. Although these experiments do not include provisions for direct drag measurement, boundary-layer measurements are used to estimate drag and skin-friction coefficients following the method of Fransson & Talamelli (2012). An analysis is conducted in two parts: quantifying drag induced by roughness and estimating the length of transition delay necessary to offset increased drag.

Using an integral form of the conservation-of-momentum equation as in Schlichting (1979), the following expression results for τ_w:

$$\frac{\tau_w}{\rho U_\infty} = \frac{\mathrm{d}\theta}{\mathrm{d}x} + \frac{1}{U_\infty}\frac{\mathrm{d}U_\infty}{\mathrm{d}x}\left(\delta^* + 2\theta\right). \tag{4.1}$$

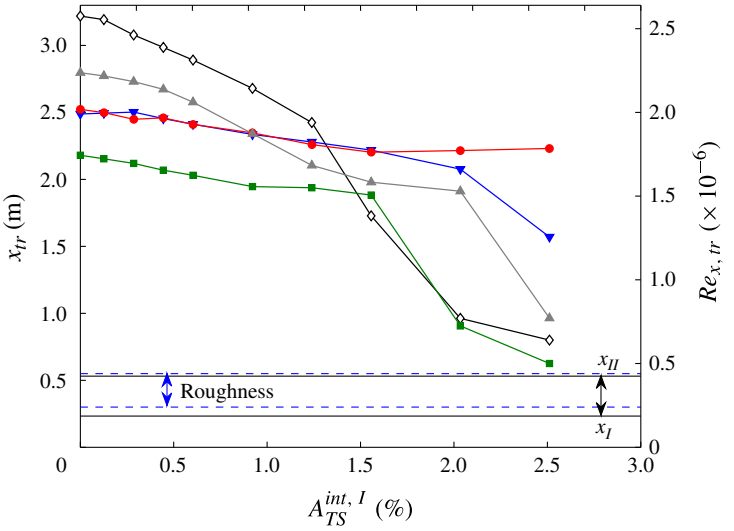

FIGURE 17. (Colour online) Transition location as a function of initial forcing amplitude for the reference case (◊), and for $L = 250$ mm, $\lambda = 10$ mm (■), $\lambda = 15$ mm (▼), $\lambda = 20$ mm (●), $\lambda = 30$ mm (▲). The flow is $U_\infty = 12$ m s^{-1} with $F = 120$. Solid horizontal lines mark the TS-growth region, and dashed lines mark the streamwise extent of the roughness field.

With the exception of the leading-edge region, the edge velocity in these experiments is approximately constant in x as a direct consequence of aligning the plate for zero-pressure-gradient flow. To the extent that it varies, it is estimated that the first term in this equation is 5–25 times larger than the second term at the conditions of these experiments. Thus, in this analysis, $\mathrm{d}U_\infty/\mathrm{d}x \approx 0$. Modulation of the mean flow is accounted for by integrating measured $\theta(x, z)$ values in the spanwise direction:

$$\theta^z = \int_{-1/2}^{1/2} \theta(x, z)\mathrm{d}\zeta\,. \tag{4.2}$$

To account for additional wetted surface area, it is first recognized that roughness cross-sections of width $s = 6$ mm have upper path lengths of $s_u = 6.44$ mm. Combining these expressions and assumptions, the skin-friction coefficient per metre of span is written in the following form:

$$C_f^z(x) = 2\frac{\tau_w}{\rho U_\infty^2}\left(1 + \frac{s_u - s}{\lambda}\right) = 2\frac{\mathrm{d}\theta^z}{\mathrm{d}x}\left(1 + \frac{s_u - s}{\lambda}\right). \tag{4.3}$$

Curve fits to measured values of θ^z are performed and differentiated directly, to avoid the problems associated with numerical differentiation. Due to sharp changes in $\theta^z(x)$ near the roughness leading and trailing edges, the data are fitted in three segments: upstream of the roughness, over the roughness surface and downstream of the roughness. Estimated values of C_f are plotted in figure 18, showing increased skin friction in the vicinity of the roughness field for all cases. As the roughness is ramped down to the plate surface at its trailing edge, $\theta^z(x)$ increases sharply producing the large spikes in figure 18 at $x = 550$ mm. The physical interpretation is that wake flow

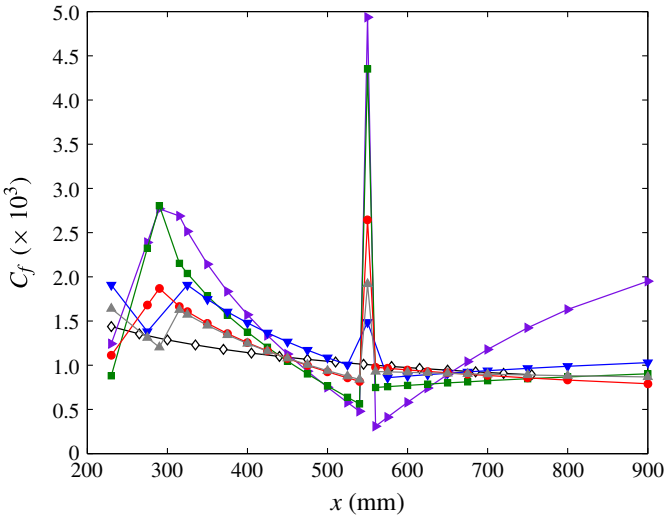

FIGURE 18. (Colour online) Skin-friction coefficient for the conditions of figure 10. Points represent the reference case (◊), and with $L = 250$ mm roughness, $\lambda = 7.5$ mm (►), $\lambda = 10$ mm (■), $\lambda = 15$ mm (▼), $\lambda = 20$ mm (●), $\lambda = 30$ mm (▲).

produces high drag. C_f values decrease as roughness-induced disturbances dissipate except in the $\lambda = 7.5$ mm case due to incipient transition, as indicated in preceding results.

To address the question of whether increased drag is offset by transition delay, the case with $A_{TS}^{int,I} = 1.1\,\%$ is considered, with and without $\lambda = 15$ mm, $L = 250$ mm roughness. Excess drag due to roughness-induced disturbances $\Delta C_{f,k}$ is estimated by integrating $C_f^z(x)$ values and subtracting drag from the reference case:

$$\Delta C_{f,k} = \int_{x_0}^{x_f} C_f^z(x)\mathrm{d}x - \int_{x_0}^{x_f} C_{f,2D}(x)\mathrm{d}x. \tag{4.4}$$

For the aforementioned case and taking $[x_0, x_f] = [230, 900]$ mm, $\Delta C_{f,k} = 0.106$ mm. As shown in figure 12, transition is delayed from 1030 to 1680 mm. At $x = 1030$ mm, values obtained from numerical differentiation show that C_f increases by nearly a factor of three: from 0.0014 to 0.004 at these conditions. If transition is delayed by approximately 41 mm at the conditions of this test case, the additional drag due to roughness is offset. Any transition delay beyond this value results in drag reduction. Thus, in this case transition is delayed nearly 15 times farther than is necessary to compensate for roughness-induced drag. Even with the approximations and assumptions made in this analysis, these data admit the possibility of a net drag reduction.

5. Discussion and conclusions

Working from the background of Fransson *et al.* (2006) and Shahinfar *et al.* (2012), a new approach is undertaken to ameliorate TS-wave growth and delay the onset of transition. This approach rests on the notion that a smooth, spanwise-periodic surface pattern may produce the steady spanwise mean-flow modulation that is required for the streak stabilization mechanism, and do so in a manner which renders the steady disturbances more robust in the sense that they are less prone to bypass transition.

The first approximation to this notional surface is a pattern of elongated roughness elements with hemispherical-cap cross-sections. The utility of this approach is that the spanwise spacing or streamwise length of the pattern is easily modified for parameter studies. Using controlled forcing of low- to moderate-amplitude TS waves, disturbance growth and transition are incited in a repeatable and quantifiable manner. For TS waves with $F = 100$ and amplitudes restricted to the linear growth regime, it is observed that a roughness pattern with $Re_k \leqslant 424$ and $\lambda = 15$ mm ($\beta = 0.26$) most effectively attenuates the amplitude of the TS waves. Although the presence of the roughness advances transition for low TS-wave amplitudes, moderate-amplitude TS waves ($A_{TS}^{rms,II} > 0.7\,\%$) which lead to secondary instability growth may be controlled successfully. That is, significant delays in the onset of transition are observed at these conditions. Extending the roughness pattern more effectively damps the TS waves, but results in a shorter transition delay. Thus, the underlying concept is validated by the present experiments.

The computations of Cossu & Brandt (2004) show that the TS waves are attenuated by negative production, or spanwise shear in the mean flow working against $\overline{u'w'}$. The antisymmetric $\partial U/\partial z$ fields are observed experimentally and this explanation appears correct. Contours of the mean flow over the roughness pattern show that it is similarly deformed, though perhaps to a somewhat smaller degree than expected. Given that significant attenuation of TS-wave amplitude is observed, it stands to reason that spanwise shear in the mean flow is the more important ingredient. In the wake of the roughness, a system of high-speed and low-speed regions modulated in z develops in a manner which is not dissimilar to the streaky boundary layers produced by conventional roughness via the lift-up mechanism. That the periodicity of the wake grows in x admits the possibility of a streak-generating mechanism, such as weak streamwise vorticity produced by the elongated roughness. In the present experiments, however, the magnitude of the streaks is less than half of that in the experiments of Shahinfar *et al.* (2013), and furthermore, amplitude attenuation is observed before the end of the roughness. Thus, this explanation appears incomplete for the present experiments.

It is worthwhile to reconsider the experiments of Grek *et al.* (1996) and the simulations of Litvinenko *et al.* (2006), in which the effect of riblets on transition was studied. Both efforts concluded that the finely spaced riblets enhance TS-wave growth rates, but more importantly, that the development of turbulent spots from Λ vortices is delayed in the presence of the riblets. Transition delay is only achieved in the present experiments when the forcing amplitude is large enough that the TS waves are reasonably expected to produce these Λ vortices. Given these observations, it is possible that lingering effects of the roughness in the boundary layer delay the onset of transition by inhibiting the formation of turbulent spots. At these moderate amplitudes, a K-type pattern is expected (Herbert 1988) in which the spanwise wavelength λ_z of these structures is about half that of the streamwise TS wavelength, λ_x. The streamwise wavelength is measured indirectly by tracking the phase of the TS waves in x which results in $\lambda_x = 28.4$ mm for these TS waves at $F = 100$. Thus, $\lambda_z \approx 14.2$ mm. It is further noted that the most effective roughness wavelengths for transition delay are 15–20 mm, or slightly longer than the estimated spanwise wavelength of the Λ vortices.

The boundary-layer measurements have revealed a shortcoming of this approach in that disturbances are amplified in the near-wake region of the elongated roughness. Furthermore, placing the trailing edge of the roughness past branch II reduces but does not eliminate this problem. Combined with the idea that the spanwise-periodic

wall shape may favourably affect the development of turbulent spots, the next step is to extend the roughness pattern to the entire length of the plate. This is closer to approximating a wavy wall, rather than a flat plate with a roughness field. Building on the parametric studies of the present experiments, the wavelength of this surface roughness pattern can be optimized for potential transition delay at specific conditions. Transition that is not forced by large-amplitude, fixed-frequency disturbances is currently untested by this streak-stabilization mechanism. The path taken to turbulent breakdown in that scenario will undoubtedly rely on receptivity of naturally present disturbances. The combined problems of natural receptivity and the presence of unstable disturbances across broad frequency bands remain to be addressed before practical application of this method is deemed viable. Furthermore, the potential application of this method to flows with elevated free-stream turbulence is also unexplored. Some hints at feasibility in these scenarios may be discerned from existing results. First, the experiments of Fransson *et al.* (2006) demonstrated a modest delay in transition forced by a signal comprising broadband random noise. Secondly, some degree of latitude in tuning roughness wavelength to forced disturbances is apparent. When MVG wavelength is fixed and disturbance frequency is varied, Shahinfar *et al.* (2013) observe transition delay across a range of frequencies. Similarly, at a fixed frequency in the present experiments, transition delay is achieved across a range of roughness wavelengths. Taken together, these observations indicate that a notional set of steady streaks induced by MVGs, a wavy surface, or other surface features are able to attenuate disturbance growth across a range of frequencies or speeds. That naturally arising disturbances are unstable about a range of temporal frequencies does not therefore preclude the possibility of control by a passive mechanism.

The stated goal of the present work is to develop and investigate a new method for passive drag reduction in a flat-plate boundary layer. The results of earlier experimental and computational studies of roughness-induced transition and roughness interactions with TS waves guide this work, where the roughness may be random and distributed, or arrays of discrete features such as short cylinders, MVGs, or riblets. A prototypical wavy wall is approximated using long, regularly spaced humps to form a surface pattern. Compared with smooth-wall cases with forced TS waves, the streamwise extent of laminar flow is increased by up to 70 % in the corresponding rough-wall cases. Though forced moderate-amplitude TS waves are somewhat unrealistic, unforced transition in low-turbulence environments such as that encountered in flight can result from naturally arising TS waves. Before a real application can be considered, control of low-amplitude TS waves must first be demonstrated. Future experimental work will move beyond this proof-of-concept to a more aerodynamically simple rough wall shape, with broadband unsteady disturbances more representative of natural perturbations as this research marches toward the ultimate goal of demonstrating passive drag reduction via delay of natural transition.

Acknowledgements

This research is part of the AFRODITE project, and is supported financially by the European Research Council. The authors acknowledge the assistance of S. S. Sattarzadeh with setting up the base flow and disturbance forcing system. The assistance of B. Fallenius and J. Karlström in manufacturing the roughness elements is also appreciated.

REFERENCES

ANDERSSON, P., BERGGREN, M. & HENNINGSON, D. S. 1999 Optimal disturbances and bypass transition in boundary layers. *Phys. Fluids* **11** (1), 134–150.

ANDERSSON, P., BRANDT, L., BOTTARO, A. & HENNINGSON, D. S. 2001 On the breakdown of boundary layer streaks. *J. Fluid Mech.* **428**, 29–60.

BAGHERI, S. & HANIFI, A. 2007 The stabilizing effect of streaks on Tollmien–Schlichting and oblique waves: a parametric study. *Phys. Fluids* **19** (7), 078103.

BAKE, S., FERNHOLZ, H. H. & KACHANOV, Y. S. 2000 Resemblance of K- and N-regimes of boundary-layer transition at late stages. *Eur. J. Mech. (*B*/Fluids)* **19** (1), 1–22.

BAKE, S., KACHANOV, Y. S. & FERNHOLZ, H. H. 1996 Subharmonic K-regime of boundary-layer breakdown. In *Transitional Boundary Layers in Aeronautics* (ed. R. A. W. M. Henkes & J. L. van Ingen), North-Holland.

BECHERT, D. W., BRUSE, M., HAGE, W., VAN DER HOEVEN, J. G. T. & HOPPE, G. 1997 Experiments on drag-reducing surfaces and their optimization with an adjustable geometry. *J. Fluid Mech.* **338**, 59–87.

BENNETT, J. & HALL, P. 1988 On the secondary instability of Taylor–Görtler vortices to Tollmien–Schlichting waves in fully developed flows. *J. Fluid Mech.* **186**, 445–469.

BORODULIN, V. I., GAPONENKO, V. R., KACHANOV, Y. S., MEYER, D. G. W., RIST, U., LIAN, Q. X. & LEE, C. B. 2002*a* Late-stage transitional boundary-layer structures. Direct numerical simulation and experiment. *Theor. Comput. Fluid Dyn.* **15** (5), 317–337.

BORODULIN, V. I., KACHANOV, Y. S. & KOPTSEV, D. B. 2002*b* Experimental study of resonant interactions of instability waves in a self-similar boundary layer with an adverse pressure gradient: I. Tuned resonances. *J. Turbul.* **3** (62), 1–38.

CORKE, T. C., BAR-SEVER, A. & MORKOVIN, M. V. 1986 Experiments on transition enhancement by distributed roughness. *Phys. Fluids* **29** (10), 3199–3213.

COSSU, C. & BRANDT, L. 2004 On Tollmien–Schlichting-like waves in streaky boundary layers. *Eur. J. Mech. (*B*/Fluids)* **23** (6), 815–833.

DENISSEN, N. A. & WHITE, E. B. 2013 Secondary instability of roughness-induced transient growth. *Phys. Fluids* **25** (11), 114108.

VON DOENHOFF, A. E. & HORTON, E. A. 1958 A low-speed experimental investigation of the effect of a sandpaper type of roughness on boundary-layer transition. *NACA Tech. Rep.* 1349.

ERGIN, F. G. & WHITE, E. B. 2006 Unsteady and transitional flows behind roughness elements. *AIAA J.* **44** (11), 2504–2514.

FRANSSON, J. H. M., BRANDT, L., TALAMELLI, A. & COSSU, C. 2004 Experimental and theoretical investigation of the nonmodal growth of steady streaks in a flat plate boundary layer. *Phys. Fluids* **16** (10), 3627–3638.

FRANSSON, J. H. M., BRANDT, L., TALAMELLI, A. & COSSU, C. 2005*a* Experimental study of the stabilization of Tollmien–Schlichting waves by finite amplitude streaks. *Phys. Fluids* **17** (5), 054110.

FRANSSON, J. H. M., MATSUBARA, M. & ALFREDSSON, P. H. 2005*b* Transition induced by free-stream turbulence. *J. Fluid Mech.* **527**, 1–25.

FRANSSON, J. H. M. & TALAMELLI, A. 2012 On the generation of steady streamwise streaks in flat-plate boundary layers. *J. Fluid Mech.* **698**, 211–234.

FRANSSON, J. H. M., TALAMELLI, A., BRANDT, L. & COSSU, C. 2006 Delaying transition to turbulence by a passive mechanism. *Phys. Rev. Lett.* **96** (6), 064501.

GAPONENKO, V. R. & KACHANOV, Y. S. 1994 New methods of generation of controlled spectrum instability waves in the boundary layers. In *7th International Conference on the Methods of Aerophysical Research. Proceedings. Part 1*, pp. 90–97. Inst. Theor. & Appl. Mech.

GARCÍA-MAYORAL, R. & JIMÉNEZ, J. 2011*a* Drag reduction by riblets. *Phil. Trans. R. Soc. Lond.* A **369** (1940), 1412–1427.

GARCÍA-MAYORAL, R. & JIMÉNEZ, J. 2011*b* Hydrodynamic stability and breakdown of the viscous regime over riblets. *J. Fluid Mech.* **678**, 317–347.

GARZON, G. A. & ROBERTS, M. W. 2013 Effect of a small surface wave on boundary-layer transition. *AIAA Paper* 2013-3110.

GREEN, J. E. 2008 Laminar flow control – back to the future? *AIAA Paper* 2008-3738.

GREK, G. R., KOZLOV, V. V. & TITARENKO, S. V. 1996 An experimental study of the influence of riblets on transition. *J. Fluid Mech.* **315**, 31–49.

GREK, G. R., KOZLOV, V. V., TITARENKO, S. V. & KLINGMANN, B. G. B. 1995 The influence of riblets on a boundary layer with embedded streamwise vortices. *Phys. Fluids* **7** (10), 2504–2506.

GÜRÜN, A. M. & WHITE, E. B. 2005 Tollmien–Schlichting wave suppression and transition delay using stationary transient disturbances. *AIAA Paper* 2005-5313.

HALL, P. & BENNETT, J. 1986 Taylor–Görtler instabilities of Tollmien–Schlichting waves and other flows governed by the interactive boundary-layer equations. *J. Fluid Mech.* **171**, 441–457.

HERBERT, T. 1988 Secondary instability of boundary layers. *Annu. Rev. Fluid Mech.* **20**, 487–526.

JOHANSSON, A. V. & ALFREDSSON, P. H. 1982 On the structure of turbulent channel flow. *J. Fluid Mech.* **122**, 295–314.

KACHANOV, Y. S. 1994 Physical mechanisms of laminar-boundary-layer transition. *Annu. Rev. Fluid Mech.* **26**, 411–482.

KLEBANOFF, P. S., CLEVELAND, W. G. & TIDSTROM, K. D. 1992 On the evolution of a turbulent boundary layer induced by a three-dimensional roughness element. *J. Fluid Mech.* **237**, 101–187.

KLEBANOFF, P. S., TIDSTROM, K. D. & SARGENT, L. M. 1962 The three-dimensional nature of boundary-layer instability. *J. Fluid Mech.* **12** (1), 1–34.

KLUMPP, S., MEINKE, M. & SCHRÖDER, W. 2010 Numerical simulation of riblet controlled spatial transition in a zero-pressure-gradient boundary layer. *Flow Turbul. Combust.* **85** (1), 57–71.

KOSORYGIN, V. S., RADEZTSKY, R. H. & SARIC, W. S. 1995 Laminar boundary-layer, sound receptivity and control. In *Laminar-Turbulent Transition IV* (ed. R. Kobayashi), pp. 517–524. Springer.

LADD, D. M., ROHR, J. J., REIDY, L. W. & HENDRICKS, E. W. 1993 The effect of riblets on laminar to turbulent transition. *Exp. Fluids* **14** (1–2), 1–9.

LANDAHL, M. T. 1980 A note on an algebraic instability of inviscid parallel shear flows. *J. Fluid Mech.* **98** (2), 243–251.

LINDGREN, B. & JOHANSSON, A. V. 2002 Evaluation of the flow quality in the MTL wind-tunnel. *Tech. Rep.* TRITA-MEK 2002:13. KTH Mechanics, Stockholm.

LITVINENKO, Y. A., CHERNORAY, V. G., KOZLOV, V. V., LOEFDAHL, L., GREK, G. R. & CHUN, H. H. 2006 The influence of riblets on the development of a Λ structure and its transformation into a turbulent spot. *Dokl. Phys.* **51** (3), 144–147.

LIU, Y., ZAKI, T. A. & DURBIN, P. A. 2008 Floquet analysis of secondary instability of boundary layers distorted by Klebanoff streaks and Tollmien–Schlichting waves. *Phys. Fluids* **20** (12), 124102.

LUCHINI, P. 2000 Reynolds-number-independent instability of the boundary layer over a flat surface: optimal perturbations. *J. Fluid Mech.* **404**, 289–309.

LUCHINI, P. & TROMBETTA, G. 1995 Effects of riblets upon flow stability. *Appl. Sci. Res.* **54** (4), 313–321.

MALIK, M. R. & HUSSAINI, M. Y. 1990 Numerical simulation of interactions between Görtler vortices and Tollmien–Schlichting waves. *J. Fluid Mech.* **210**, 183–199.

MENDONÇA, M. T., MORRIS, P. J. & PAULEY, L. L. 2000 Interaction between Görtler vortices and two-dimensional Tollmien–Schlichting waves. *Phys. Fluids* **12** (6), 1461–1471.

MORKOVIN, M. V. 1969 On the many faces of transition. In *Viscous Drag Reduction* (ed. C. S. Wells), Plenum.

NAYFEH, A. H. 1981 Effect of streamwise vortices on Tollmien–Schlichting waves. *J. Fluid Mech.* **107**, 441–453.

NAYFEH, A. H. & AL-MAAITAH, A. 1988 Influence of streamwise vortices on Tollmien–Schlichting waves. *Phys. Fluids* **31** (12), 3543–3549.

NAYFEH, A. H. & ASHOUR, O. N. 1994 Acoustic receptivity of a boundary layer to Tollmien–Schlichting waves resulting from a finite-height hump at finite Reynolds numbers. *Phys. Fluids* **6** (11), 3705–3716.

NUGROHO, B., HUTCHINS, N. & MONTY, J. P. 2013 Large-scale spanwise periodicity in a turbulent boundary layer induced by highly ordered and directional surface roughness. *Intl J. Heat Fluid Flow* **41**, 90–102.

PELTZER, I. 2008 Comparative in-flight and wind tunnel investigation of the development of natural and controlled disturbances in the laminar boundary layer of an airfoil. *Exp. Fluids* **44** (6), 961–972.

PRESS, W. H., TEUKOLSKY, S. A., VETTERLING, W. T. & FLANNERY, B. P. 2007 *Numerical Recipes: The Art of Scientific Computing*, 3rd edn. Cambridge University Press.

RESHOTKO, E. 2001 Transient growth: a factor in bypass transition. *Phys. Fluids* **13** (5), 1067–1075.

RESHOTKO, E., SARIC, W. S. & NAGIB, H. M. 1997 Flow quality issues for large wind tunnels. *AIAA Paper* 97-0225.

RIEDEL, H. & SITZMANN, M. 1998 In-flight investigations of atmospheric turbulence. *Aerosp. Sci. Technol.* **2** (5), 301–319.

RUBAN, A. I. 1984 On the generation of Tollmien–Schlichting waves by sound. *Fluid Dyn.* **19** (5), 709–717.

RUBAN, A. I., DUCK, P. W. & ZHIKHAREV, C. N. 1996 The generation of Tollmien–Schlichting waves by freestream vorticity perturbations. *AIAA Paper* 96-2123.

SARIC, W. S. 1994 Görtler vortices. *Annu. Rev. Fluid Mech.* **26**, 379–409.

SARIC, W. S. 2007 Boundary-layer stability and transition. In *Springer Handbook of Experimental Fluid Mechanics* (ed. C. Tropea, A. L. Yarin & J. F. Foss), pp. 886–896. Springer.

SARIC, W. S., CARPENTER, A. L. & REED, H. L. 2011 Passive control of transition in three-dimensional boundary layers, with emphasis on discrete roughness elements. *Phil. Trans. R. Soc. Lond.* A **369** (1940), 1352–1364.

SARIC, W. S., CARRILLO, R. B. & REIBERT, M. S. 1998 Nonlinear stability and transition in 3-D boundary layers. *Meccanica* **33** (5), 469–487.

SARIC, W. S., REED, H. L. & KERSCHEN, E. J. 2002 Boundary-layer receptivity to freestream disturbances. *Annu. Rev. Fluid Mech.* **34**, 291–319.

SCHLATTER, P., DEUSEBIO, E., DE LANGE, R. & BRANDT, L. 2010 Numerical study of the stabilisation of boundary-layer disturbances by finite amplitude streaks. *Intl J. Flow Control* **2** (4), 259–288.

SCHLICHTING, H. 1979 *Boundary-Layer Theory*, 7th edn. McGraw-Hill.

SCHUELE, C. Y., CORKE, T. C. & MATLIS, E. 2013 Control of stationary cross-flow modes in a Mach 3.5 boundary layer using patterned passive and active roughness. *J. Fluid Mech.* **718**, 5–38.

SHAHINFAR, S., FRANSSON, J. H. M., SATTARZADEH, S. S. & TALAMELLI, A. 2013 Scaling of streamwise boundary layer streaks and their ability to reduce skin-friction drag. *J. Fluid Mech.* **733**, 1–32.

SHAHINFAR, S., SATTARZADEH, S. S. & FRANSSON, J. H. M. 2014 Passive boundary layer control of oblique disturbances by finite-amplitude streaks. *J. Fluid Mech.* **749**, 1–36.

SHAHINFAR, S., SATTARZADEH, S. S., FRANSSON, J. H. M. & TALAMELLI, A. 2012 Revival of classical vortex generators now for transition delay. *Phys. Rev. Lett.* **109** (7), 074501.

STRAND, J. S. & GOLDSTEIN, D. B. 2011 Direct numerical simulations of riblets to constrain the growth of turbulent spots. *J. Fluid Mech.* **668**, 267–292.

USTINOV, M. V. 1995 Secondary instability modes generated by a Tollmien–Schlichting wave scattering from a bump. *Theor. Comput. Fluid Dyn.* **7** (5), 341–354.

WHITE, E. B. 2002 Transient growth of stationary disturbances in a flat plate boundary layer. *Phys. Fluids* **14** (12), 4429–4439.

WHITE, E. B. & ERGIN, F. G. 2004 Using laminar-flow velocity profiles to locate the wall behind roughness elements. *Exp. Fluids* **36** (5), 805–812.

WU, X. 2001 Receptivity of boundary layers with distributed roughness to vortical and acoustic disturbances: a second-order asymptotic theory and comparison with experiments. *J. Fluid Mech.* **431**, 91–133.

ZVERKOV, I., ZANIN, B. & KOZLOV, V. 2008 Disturbances growth in boundary layers on classical and wavy surface wings. *AIAA J.* **46** (12), 3149–3158.